Geochemistry of olivine-hosted melt inclusions in the Baekdusan (Changbaishan) basalts: Implications for recycling of oceanic crustal materials into the mantle source

Hyun-Ok Cho, Sung Hi Cho, Pierre Schiano, Moonsup Cho, Nicolas Cluzel, Jean-Luc Devidal, Kyoochul Ha

Geochemistry of olivine-hosted melt inclusions in the Baekdusan (Changbaishan) basalts: Implications for recycling of oceanic crustal materials into the mantle source

Hyun-Ok Choi[a], Sung Hi Choi[a,b,*], Pierre Schiano[c], Moonsup Cho[d], Nicolas Cluzel[c], Jean-Luc Devidal[c], Kyoochul Ha[e]

[a] Department of Astronomy, Space Science and Geology, Chungnam National University, Daejeon 34134, South Korea

[b] Department of Geology and Earth Environmental Sciences, Chungnam National University, Daejeon 34134, South Korea

[c] Laboratoire Magmas et Volcans, Université Blaise Pascal – CNRS – IRD, 6 avenue Blaise Pascal, 63178 Aubière, France

[d] School of Earth and Environmental Sciences, Seoul National University, Seoul 08826, South Korea

[e] Geological Environmental Division, Korea Institute of Geoscience and Mineral Resources, Daejeon 34132, South Korea

*Corresponding author: chois@cnu.ac.kr (Tel.: +82 42 821 6428; Fax: +82 42 821 8861)

ABSTRACT

We determined the major and trace element concentrations of olivine-hosted melt inclusions in basalts from the active Baekdusan volcano situated on the border between China and North Korea in order to understand better the nature of the mantle source and the geodynamic processes that gave rise to volcanism at this site. Rehomogenized melt inclusions (after 'Fe-loss' correction) can be divided into three groups: a low-Si alkaline group, a high-

Si alkaline group, and a high-Si sub-alkaline group. The low-Si group is composed of picrobasalt to basanite, and the high-Si group consists of (trachy)basalt to basaltic (trachy)andesite. The low-Si group has generally higher TiO_2, CaO, and P_2O_5, but lower Al_2O_3, Na_2O, and K_2O contents at a given MgO concentration compared with those in the high-Si group. The CaO and P_2O_5 contents are positively correlated, indicating the presence of a calcium phosphate, probably tuite [γ-$Ca_3(PO_4)_2$], in the source. The melt inclusions are enriched in light rare earth elements [$(La/Yb)_N$ = 7.8–30.4]. On a primitive-mantle-normalized incompatible element plot, the low-Si group has positive anomalies in Ba and P compared with typical oceanic island basalt (OIB). On the other hand, the high-Si group exhibits remarkable positive anomalies in Eu, Ba, Rb, K, Pb, P, and Ti, implying that K-hollandite and tuite are essential phases in the source. The high-Si subalkaline group has lower abundances of incompatible elements than the high-Si alkaline group, reflecting different degrees of partial melting from the same source. In contrast to OIB, Baekdusan magmatism is characterized by positively fractionated $(Zr/Hf)_N$ ratios, and is best approximated by admixture of partial melts derived from both clinopyroxene-rich eclogite and garnet peridotite. Intraplate volcanism in northeastern Asia is closely associated with deep subduction of the Pacific plate. The subducting Pacific slab flattens and stagnates in the mantle transition zone under northeastern Asia, and this zone may yield a wet plume. Focused mantle upwelling through a gap in the stagnant slab may also be accompanied to the plume responsible for the Baekdusan magmatism. Thermal decomposition of K-hollandite within recycled continent-derived sediments is likely to metasomatize the ambient mantle peridotite above the stagnant slab. As the plume ascends through the upper mantle, the metasomatized mantle and recycled oceanic crustal materials (tuite-bearing eclogite or garnet pyroxenite) entrained by the plume may undergo partial melting, resulting in the volcanism observed at Baekdusan.

Keywords: Baekdusan, mantle transition zone, melt inclusions in olivine phenocrysts, recycled oceanic crustal materials, plume

1. Introduction

Silicate melt inclusions (hereafter 'melt inclusions') are small droplets entrapped in phenocrysts during their growth within magmatic systems (e.g., Lowenstern, 1995; Roedder, 1984). Melt inclusions entrapped by phenocrysts that formed early in the process of magma evolution may represent snapshots of primitive magmatic conditions (Kent, 2008; Schiano, 2003; Shimizu, 1998; Sobolev, 1996). Studies of such melt inclusions can provide important insights into the nature of mantle sources and the melting and melt transport processes that occur in primitive magma and are subsequently erased from the basaltic rock by fractional crystallization, magma mixing, or crustal contamination during its evolution. Meanwhile, it is well recognized that the original composition of a melt inclusion may be altered by post-entrapment processes during natural cooling, such as crystallization of host minerals on the walls of inclusions, crystallization of other daughter minerals inside the inclusions, formation of shrinkage bubbles, or diffusive re-equilibration between host minerals and the external magma (e.g., Chen et al., 2011; Cottrell et al., 2002; Danyushevsky et al., 2000; Gaetani and Watson, 2000; Qin et al., 1992; Roedder, 1984). Such modification, however, can be reversed by rehomogenization experiments and/or numerical reconstruction (e.g., Danyushevsky et al., 2002; Kent, 2008; Schiano, 2003).

Late Cenozoic intraplate volcanism is widespread in the eastern North China Craton (NCC; Fig. 1a, b). Numerous petrological and geochemical studies have shown that Cenozoic basaltic rocks have oceanic island basalt (OIB)-like patterns of trace element distribution, including enrichment of light rare earth elements (LREE) and a lack of depletion of high field strength elements (HFSE), and thus might be derived from a peridotitic source in the subcontinental lithospheric mantle or asthenosphere (Basu et al., 1991; Chen et al., 2003; Chu et al., 2013; Kuritani et al., 2009, 2013; Li et al., 2014; Sakuyama et al., 2013; Xu et al., 2005, 2012a; Yan and Zhao, 2008; Zhang et al., 1995, 2015; Zou et al., 2008). However, there is a general consensus that the peridotitic source contains a significant proportion of mafic lithologies such as pyroxenite, eclogite, or hornblendite, which may play an important role in generating OIB-like intraplate basaltic magmatism (e.g., Eisele et al., 2002; Gao et al., 2004, 2008; Hauri, 1996; Hirschmann et al., 2003; Keshav et al., 2004; Kogiso et al., 2003; Kogiso and Hirschmann, 2006; Pertermann and Hirschmann, 2003a, b; Rehkämper and Hofmann, 1997; Sobolev et al., 2005, 2007; Yaxley and Green, 1998). Recycled oceanic crust or melt-peridotite reaction products may provide the mafic source rocks (e.g., Hauri, 1996; Herzberg, 2011; Sobolev et al., 2005, 2007; Straub et al., 2008), and some Cenozoic basaltic rocks from the eastern NCC (e.g., Abaga-Dalinuoer, Chifeng, Jilin, Hebei, Hannuoba, Liaoning, Bohai Bay, Shandong, Anhui, Jiangsu) may be derived from a source lithology containing pyroxenite in addition to peridotite (Hong et al., 2013; Li et al., 2016; Liu et al., 2008; Qian et al., 2015; Zhang et al., 2009; Zhang and Guo, 2016).

The Baekdusan volcanic field (also called Changbaishan in China; N41°20′–42°40′, E127°00′–129°00′), located on the border between China and North Korea, represents the largest exposure of intraplate volcanic rocks on the NCC (Fig. 1b, c). The volcanoes in this area have erupted repeatedly in historical times. The most powerful eruption, called “the Millennium Eruption”, occurred with a Volcanic Explosivity Index (VEI) of 6 or 7 in ca.

938–946 AD (Horn and Schmincke, 2000; Iacovino et al., 2016; Wei et al., 2013; Xu et al., 2013; Yin et al., 2012; Zou et al., 2010). Voluminous Plinian fallout, ignimbrite, lahar, and other erupted materials covered 33,000 km^2 of northeastern China and Korea (Stone, 2011; Sun et al., 2014), and extended as far as northern Japan, ~1200 km from the volcano (Machida and Arai, 1983). After the Millennium Eruption, minor volcanic activity continued, with eruptions in 1413, 1597, 1668, 1702, 1898, and 1903 AD, exhibiting a roughly 100-year periodicity (Cui et al., 1995; Stone, 2011; Xu et al., 2012b, 2013). Although the volcano has not erupted in the past 100 years, all available geological data including seismicity, ground deformation, and geochemical monitoring of springs indicate that Baekdusan is an active volcano with the potential for eruption in the near future (Ramos et al., 2016; Wei et al., 2003, 2013; Xu et al., 2012b; Yun and Lee, 2012). Thus, it is of the utmost importance to understand the nature of the magmatism to anticipate its behaviour at this site. Previous studies have primarily focused on the history of Baekdusan volcanic activity (Wei et al., 2003, 2007, 2013), magma evolution and the eruptive mechanism (Liu et al., 2015a; Wang et al., 2003; Zhang et al., 2015; Zou et al., 2008, 2010, 2014), and geochemical lines of evidence of enriched mantle sources (Basu et al., 1991; Chen et al., 2007; Hsu et al., 2000; Kuritani et al., 2009; Liu et al., 2015a). Here, we describe for the first time the major and trace element compositions of re-heated melt inclusions entrapped in olivine phenocrysts from the Baekdusan basaltic rocks. Combining these data with whole-rock major element, trace element, and host olivine compositions, we shed light on (1) the particular mineral phases and lithologies of the mantle source, (2) the nature of source heterogeneities, and (3) the geodynamic processes that gave rise to volcanism at Baekdusan.

2. Geological setting and sampling

The NCC is one of the oldest cratons in the world (~3.8 Ga; Liu et al., 1992; Zheng et al., 2004), and the Baekdusan volcanic field is located on the northeastern margin of the NCC (Fig. 1a, b). The basement of the eastern NCC consists primarily of Archean tonalite-trondhjemite-granodiorite (TTG) gneisses, granitoids, and supracrustal rocks, which are locally overlain by Proterozoic to Paleozoic strata (e.g., Wang et al., 2003, Zhang et al., 2015, 2017). The eastern NCC experienced widespread tectonothermal reactivation during the Late Mesozoic to Cretaceous, as indicated by the emplacement of voluminous silicic intrusions and volcanic rocks (e.g., Meng, 2003). The Central Asian Orogenic Belt (CAOB; Fig. 1a) bounds the NCC to the north. Disappearance of the Paleo-Asian Ocean between the NCC and the southern accretionary margin of the Siberian Craton was completed in the Late Paleozoic to Early Mesozoic (Eizenhöfer et al., 2014), and the paleo-Pacific plate began to subduct under the Asian continent in the Early Jurassic (Sun et al., 2013). The Baekdusan volcanic field lies ~1,300 km away from the Japan Trench. Recent studies of seismic tomography show that the subducting Pacific slab flattens and stagnates in the mantle transition zone (~410 to 660 km depth) under northeastern Asia (Duan et al., 2009; Guo et al., 2016; Huang and Zhao, 2006; Lei and Zhao, 2005; Liu et al., 2015b; Zhao et al., 2009). The leading edge of the stagnant slab reaches a longitude of 120^{o}E (e.g., Huang and Zhao, 2006).

The Baekdusan field has >100 volcanic centers, including three main mountains: Tianchi in the China-North Korea border region, Wangtian'e in China, and Namphothe in North Korea (Fig. 1c). Tianchi is the youngest and tallest cone with a 5-km-wide and 384-m-deep crater lake at its summit. These mountains are the source of the headwaters of the Songhua, Yalu, and Tumen Rivers (Fig. 1b). The eruptions of these three volcanoes are geochemically indiscernible (e.g., Liu et al., 2015a), and the volcanoes each consist of an early-stage basaltic plateau, a middle-stage trachytic cone, and a late-stage explosive comenditic ignimbrite (Liu et al., 2015a; Wei et al., 2003, 2007, 2013) (Fig. 1c). The main

early shield-forming eruptions took place between 22.6 and 1.5 Ma (Wei et al., 2007, 2013), and the cone-construction stage lasted from ~1.0 Ma to ~20 ka, followed by mostly comenditic eruptions (Wei et al., 2013). Eruption of trachytic and comenditic magmas reflects a long period of differentiation from the parent basaltic magma (e.g., Wei et al., 2007).

Samples used in this study were collected from Wangtian'e volcano and Tianchi volcano along the Tumen River (Fig. 1b, c). The K-Ar whole-rock ages for the basalts range from ca. 5.5 to 0.2 Ma (Fan et al., 2007). Most samples exhibit a porphyritic texture with plagioclase phenocrysts (>0.1 mm in size) in a groundmass of olivine, clinopyroxene, plagioclase, ilmenite, and/or titanomagnetite. One sample (BDH-01) contains large olivine and plagioclase phenocrysts (up to 2–3 mm in size) in a groundmass of olivine, clinopyroxene, and plagioclase. Melt inclusions are randomly distributed throughout the olivine grains, and are generally rounded ellipsoidal shapes ~20 to ~200 μm in size. We carefully selected melt inclusions far from crack planes, which usually contain a shrinkage bubble and daughter minerals grown from the trapped melt during slow cooling.

3. Analytical procedures

All samples used in this study were freshly collected. Samples for the whole-rock analysis were crushed into small pieces (< 5 mm in diameter) in a tungsten carbide mortar, and cleaned in an ultrasonic bath containing Milli-Q water. Fresh fragments were pulverized in an agate ball mill prior to geochemical analysis. Whole-rock major element contents were analyzed by X-ray fluorescence spectrometry (XRF) at Pukyong National University in Pusan, South Korea. The data were reduced using a weighted regression line created from standards BIR-1 and MO-5. The precision of the technique for preparing and analyzing

standards was within 5% (Table S1). Whole-rock trace element concentrations were determined using inductively coupled plasma mass spectrometry (ICP-MS) at Act Labs, Ontario, Canada. Precision was estimated to be ±10% based on replicate analyses of international rock standards (BIR-1, JR-1, and DNC-1; Table 1).

Heating experiments were conducted at the Laboratoire Magmas et Volcans (Clermont-Ferrand, France) with a Vernadsky-type heated microscope stage (Sobolev et al., 1980) to determine the composition of melt at the time of its entrapment. The contents of the inclusion (glass, gas, and daughter minerals) were homogenized by heating the host olivines in a 6-mm-long vertical $Pt_{90}Rh_{10}$ tube in a purified He atmosphere under redox conditions that correspond to the iron-wüstite buffer. The temperature was monitored by a Pt-$Pt_{90}Rh_{10}$ thermocouple welded to the sample holder. The accuracy of the temperature measurements was approximately ± 20ºC, and the system was calibrated at the melting temperature of Au (1064ºC). All experiments were performed with heating rates of 0.9ºC/s from 20ºC to 900ºC and 0.4ºC/s for T > 900ºC in order to access the effects caused by variations in the rate of the transformations in the inclusions. The homogenization temperatures of melt inclusions varied from 1216ºC to 1313ºC (Table S2). After quenching, the samples were polished to expose the inclusions for electron microprobe analyses. Textural evidence of quench crystallization was absent in back-scattered electron images of the inclusions studied. Some homogenized melt inclusions, however, contain tiny sulfide globules (Fig. S1).

Major element concentrations of homogenized melt inclusions and host olivines were determined using a CAMECA SX-100 electron microprobe at the Laboratoire Magmas et Volcans. Analyses for glass samples were performed using an accelerating voltage of 15 kV and a probe current of 8 nA for major elements (Na, Al, Si, Ca, Fe, Mg, Ti, Mn, K, and P) and 80 nA for S, with a defocused (5–10 μm) beam. For host minerals, the beam size was 1 μm and the beam current was 15 nA. Counting time was 10 s for peaks and 5 s for the

background. Sulfur was analyzed in integrated mode, using 5 steps of 10 s each. The detection limit for S was ~50 ppm and analytical uncertainties were better than 10%. Natural and synthetic minerals and oxides were used for routine calibration, except for S, which was calibrated to VG2 basaltic glass according to the Smithsonian Microbeam Standards. For the glass analysis, an inter-laboratory check was performed using the international glass standard A99 (Kilauea basalt glass; Jarosewich et al., 1979; Thornber et al., 2002). These results are provided in Tables S2 and S3.

Trace element concentrations of reheated melt inclusions were analyzed by laser ablation inductively coupled plasma mass spectrometry (LA-ICP-MS) at the Laboratoire Magmas et Volcans. This instrument comprises an Excimer ArF laser (193 nm) coupled with an Agilent 7500 CS quadrupole mass spectrometer. A spot size smaller than the area of each exposed inclusion was used for analysis, which varied from 10 to 20 µm. The laser pulsed at 2 Hz, and data acquisition time was 30 s for background and 60 s for peaks. Before melt inclusion ablation and after every five batches, the reference materials NIST-610 and NIST-612 were analyzed to test for and correct any signal variation. The United States Geological Survey (USGS) Basalt of Columbia River (BCR) glass standard was analyzed as an unknown to check the accuracy of the analysis. The calibration values for NIST-610 and NIST-612 used in data reduction were from Gagnon et al. (2008). Trace element concentrations were corrected for variations in ablation efficiency between samples and standards using minor isotopes of Ca (^{43}Ca and ^{44}Ca) as an internal standard. CaO concentrations in the melt inclusions had been determined previously using an electron microprobe. Multiple analyses of BCR indicated that analytical reproducibility and accuracy were better than 10% for most reported elements. No corrections for interfering molecular or isobaric species were required due to the selection of appropriate analytical isotopes and minimal formation of molecular species, with $^{+}$ThO/$^{+}$Th <0.5% (Table S4).

4. Results and interpretation

4.1. Host basaltic rocks

Major and trace element concentrations in the host rocks are given in Table S1. On a total alkali versus silica (TAS) diagram (Le Maitre et al., 1989) (Fig. 2), they are compositionally basalt to basaltic andesite, belonging to the sub-alkaline suite. The host rocks have a limited range of SiO_2 (51.1–52.3 wt%) with Mg#s [=100Mg/(Mg+Fe^{2+})] varying from 46.0 to 59.0 (Table S1; Fig. 3). The Ni, Co, and Cr contents of the samples were 50–110, 34–39, and 70–150 ppm, respectively (Table S1). The Mg# and the Ni and Cr contents of the host basaltic rocks were lower than those of primitive basalt (Mg# >70; Ni >250–350 ppm, Cr > 500–600 ppm; Ulmer, 1989; Wilkinson and Le Maitre, 1987), reflecting fractionation of ferromagnesian minerals such as olivine and clinopyroxene. They exhibit a light rare earth element (LREE)-enriched pattern [$(La/Yb)_N$ = 8.8–10.2] on chondrite-normalized REE plots (Fig. 4a and b), with a slight positive anomaly in Eu [$(Eu/Eu^*)_N$=1.1–1.2, where $(Eu^*)_N$ = $(Sm_N + Gd_N)/2$]. Extended primitive-mantle-normalized trace element patterns (also called spidergrams) are provided in Fig. 4c and d, along with the composition of typical OIBs (Sun and McDonough, 1989). The samples reveal overall enrichment in highly incompatible elements compared with less incompatible ones. They exhibit Nb and Ta enrichment relative to LREE, resembling a typical OIB (Fig. 4c and d). However, some samples have small negative anomalies in Nb and Ta (Fig. 4c and d). Furthermore, they were distinguished by marked positive anomalies in Ba and K, and possibly P, compared with the OIB (Fig. 4c and d). Also note that these host rocks have higher fractionated $(Zr/Hf)_N$ ratios than OIB (Fig. 4c and d).

4.2. Olivine phenocrysts

Olivines are present as euhedral to subhedral phenocrysts in thin section. Major element concentrations of inclusion-bearing olivines are given in Table S3. They have Fo values ranging from 71.5 to 82.7 (Fig. 5). The CaO contents range from 0.17 to 0.28 wt%, much higher than those of mantle peridotite xenoliths (CaO < 0.1 wt%; Thompson and Gibson, 2000) (Fig. 5), indicating that these olivines are phenocrysts crystallized from basaltic magmas.

4.3. Melt inclusions in olivine phenocrysts

The major element concentrations of reheated melt inclusions are presented in Table S2. Owing to their mobility, volatiles can rapidly diffuse out of inclusions when they are breached during reheating. Thus, the sulfur content was determined in order to monitor inclusion integrity during rehomogenization experiments (Nielsen et al., 1998). The S contents obtained varied from 240 to 1380 ppm (Table S2). Reported S contents of quenched mid-ocean ridge basalt (MORB) and submarine OIB (e.g., Mauna Kea, Pitcairn, Society, and Galapagos) glasses range from ~400 to 1800 ppm and ~700 to 2200 ppm, respectively (Kendrick et al., 2014; Mathez, 1976; Nielsen et al., 1998; Stolper et al., 2004; Yi et al., 2000). We note that none of the reheated inclusions reported in this study appeared to be breached based on visual inspection. However, some homogenized melt inclusions contain tiny sulfide globules (Fig. S1), which may result in artificially low S measurements when the entire melt inclusion cannot be ablated during analysis (Danyushevsky et al., 2002). To test olivine-liquid equilibria, we calculated the Mg-Fe exchange coefficient, $K_d = (Fe^{2+}/Mg)_{Ol}/(Fe^{2+}/Mg)_{Liq}$, between inclusions (Liq) and host olivines (Ol). The calculated K_d values ranged from 0.38 to 0.65, significantly higher than the nominal value of 0.30 ± 0.03 at 1 atm (Roeder and Emslie, 1970), indicating that the melt inclusions are in disequilibrium

with their host olivines. Trapped melt composition can be modified by re-equilibration with host olivines after entrapment and prior to natural quenching (Danyushevsky et al., 2000, 2002), particularly where magma cools significantly before eruption. When re-equilibration occurs, elements that are incompatible with host minerals are unlikely to be significantly exchanged, but compatible elements can be modified and the change in composition of the trapped melt is unlikely to be reversed experimentally (Cottrell et al., 2002; Danyushevsky et al., 2000; Sobolev, 1996; Spandler et al., 2007). For olivine-hosted melt inclusions, a re-equilibration process called "Fe-loss" has been recognized in several studies (e.g., Danyushevsky et al., 2000; Sobolev and Danyushevsky, 1994), whereby Fe diffuses from a melt inclusion into the host olivine while Mg diffuses from the host into the melt inclusion, increasing the K_d value. The S solubility in a melt is positively correlated with its FeO content (e.g., Mathez, 1976; Wallace and Carmichael, 1992). Therefore, the sulfide globules observed in some homogenized melt inclusions could be a consequence of Fe-loss (Danyushevsky et al., 2002). We have corrected for Fe-loss using the computer program "Petrolog3" introduced by Danyushevsky and Plechov (2011). This calculation requires an independent estimate of the initial FeO* contents of melt inclusions. The FeO* contents of Baekdusan basalts do not show a meaningful variation attributed to magmatic differentiation (Fig. S2). We thus assumed the initial FeO* contents of melt inclusions to be a mean value of the host basaltic rocks. The Fe_2O_3 contents of trapped melts were calculated using $(Fe^{2+}/Fe^{3+})_{melt} = 9$. Corrected melt compositions are reported in Table S5. The K_d (Fe^{2+}-Mg) values between host olivines and corrected melt inclusions are between 0.29 and 0.32 (Table S5), within the range (0.30 ± 0.03; Roeder and Emslie, 1970) determined experimentally.

The SiO_2 contents of melt inclusions range from 41.7 to 53.1 wt% (Fig. 2). Based on the SiO_2 and trace element contents (see below), we divided the melt inclusions into two groups: a low-Si group (SiO_2<45 wt%) and a high-Si group (SiO_2>45 wt%). The low-Si

group is compositionally picrobasalt to basanite in the alkaline series (Fig. 2). The high-Si group consists of (trachy)basalt to basaltic (trachy)andesite, which can be further divided into two sub-groups: an alkaline (trachy)basalt-basaltic trachyandesite group and a sub-alkaline basalt-basaltic andesite group (Fig. 2). The MgO contents of the low-Si group are limited to ~7.0 wt%, but those of the high-Si group vary from 3.8 to 7.3 wt% (Fig. 3). The low-Si group has higher TiO_2, CaO, and P_2O_5 concentrations, but lower Al_2O_3, Na_2O, and K_2O contents at a given MgO than the high-Si group (Fig. 3). The sub-alkaline group has higher SiO_2, and lower Al_2O_3, Na_2O, and K_2O contents than the alkaline group at a given MgO concentration (Fig. 3). The TiO_2, Na_2O, and K_2O contents of the high-Si group increase with decreasing MgO, but the SiO_2, Al_2O_3, CaO, and P_2O_5 contents do not correlate well with MgO (Fig. 3).

The trace element concentrations of reheated melt inclusions are given in Table S4. They exhibit LREE-enriched patterns [$(La/Yb)_N$ = 7.8–30.4] similar to a typical OIB (Table S4; Fig. 4a and b). However, most of the high-Si group are distinguished by positive Eu anomalies [$(Eu/Eu^*)_N$=1.0–1.3) compared with the OIB. Furthermore, in terms of primitive-mantle-normalized multi-element patterns (Fig. 4c and d), the high-Si group is generally similar to the host basalt, characterized by significant enrichments in Ba, Rb, K, Pb, P, and Ti, and exhibits fractionated $(Zr/Hf)_N$ ratios compared with the OIB. The low-Si group also exhibits distinctive positive anomalies in Ba and P and fractionated $(Zr/Hf)_N$ ratios, but has relatively low abundances of Ba and Rb and a significantly negative anomaly in K compared with the high-Si group or host basalt. Also note that sample BD-07-5a exhibits pronounced Nb and Ta depletion relative to LREE.

5. Discussion

5.1. Source mineralogy and lithology

Melt inclusions exhibit a wider diversity of compositions than their host basalts (Fig. 3). For example, TiO_2, K_2O, and P_2O_5 contents of melt inclusions varied from 2.4 to 5.3, 0.2 to 3.0, and 0.2 to 5.3 wt%, respectively, but those species in the host basalt are lower, from 2.1 to 3.0, 1.3 to 1.8, and 0.3 to 0.7 wt%, respectively. Significant compositional diversity has often been observed in melt inclusions from a single sample (e.g., Choi et al., 2013; Gurenko and Chaussidon, 1995; Kamenetsky et al., 1998; Kent et al., 1999; Li et al., 2016; Sobolev and Shimizu, 1993). In these cases, melt inclusions have been interpreted as sampling a range of liquids reflecting a range of source compositions, extents of melting and/or melting processes, and trapped before mixing and homogenization in magma chambers diluted or averaged them to produce the compositions of erupted lavas (Kent, 2008; Schiano, 2003; Sobolev and Shimizu, 1993).

Low-Si group melt inclusions are typified by much higher MgO and lower SiO_2 concentrations than the high-Si group or host basalts, implying that they record an early stage in the evolution of magma, prior to mixing and blending at a shallow depth. The low-Si group has notably elevated CaO and P_2O_5 contents (Fig. 3d, g), and these two elements are positively correlated (Fig. 6). Major element concentrations in the high-Si sub-alkaline group generally resemble those of the host basalts, but the high-Si alkaline group exhibits significantly higher compositional diversity (Fig. 3). MgO concentrations of the host basalts apparently lie in the middle of the compositional range of high-Si alkaline group (Fig. 3). However, this group is characterized by generally lower SiO_2 and higher TiO_2, Al_2O_3, K_2O, and P_2O_5 values at a given MgO content than host basalts (Fig. 3).

Trace element concentrations of melt inclusions may be modified by diffusive equilibration with host minerals or external melts (e.g., Kent, 2008). Diffusive exchange occurs more readily for elements with higher diffusivity in host minerals, higher partition coefficients between the host mineral and melt, and smaller melt inclusions and host minerals

(Qin et al., 1992). Olivine is a favorable host for isolation of melt inclusions from the external media, because this phase possesses minimal concentrations of most elements that characterize basaltic melt, with the exceptions of Mg, Fe, and Si (e.g., Cottrell et al., 2002; Qin et al., 1992; Sobolev, 1996). Experimental result of Cherniak (2010) suggests that timescales ranging from tens of thousands to a few million years are necessary for REE in a melt inclusion with a 50-μm radius within a 1-mm radius olivine to reach 90% re-equilibration with the external melt at a temperature of 1300°C. Note that our study is limited to inclusions (> 20 μm in size; Table S2) located at the center of host olivines (> 1 mm in size). Given that estimated times for the processes of basaltic melt formation, extraction, ascent, and residence in the crust range from ~10 to 10^5 years (Reid, 2005), it is thus likely that incompatible elements in olivine-hosted melt inclusions record the signatures of primary melts from the mantle. Despite this assumption, we use incompatible element abundances and ratios in order to minimize the possibility of any modification.

Compared with a typical OIB, high-Si group melt inclusions and host basalts exhibit significantly positive anomalies in Eu, Ba, Rb, K, and Pb (Fig. 4a, c). These anomalies are also present in near-primary (i.e., highly magnesian and low SiO_2) melts hosted in Fo-rich olivine (e.g., sample BD-07-2: Fo = 82.7; MgO = 7.3 wt%; SiO_2 = 49.5 wt%) (Fig. 4a, c), suggesting a lack of crustal contamination. K-hollandite [$KAlSi_3O_8$], a high-pressure (above ~10 GPa) polymorph of potassium feldspar, is characterized by relatively high concentrations of K, Rb, Ba, and Pb concentrations (Rapp et al., 2008; Schmidt, 1996; Urakawa et al., 1994; Wang and Takahashi, 1999; Yagi et al., 1994). The positive anomalies, along with the elevated Al_2O_3 contents of the high-Si alkaline group at a given MgO (Fig. 3c), suggest a possible presence of K-hollandite in the source (Kuritani et al., 2011).

This K-hollandite signature, however, is not present in the low-Si group (Fig. 4b, d). Instead, the low-Si group together with some high-Si alkaline group have a remarkable spike

in P (Fig. 4d). Also note that the P_2O_5 contents exhibit a positive correlation with CaO contents (Fig. 6). These observations indicate the presence of a calcium phosphate in the source. Apatite is one of the major phosphates in terrestrial rocks, including the garnet lherzolite (e.g., Konzett et al., 2012; Konzett and Frost, 2009; Murayama et al., 1986). However, experimental data and thermodynamic calculations indicate that apatite is transformed to tuite [γ-$Ca_3(PO_4)_2$] at pressures above ~8 GPa (Konzett et al., 2012; Konzett and Frost, 2009; Murayama et al., 1986; Sugiyama and Tokonami, 1987; Thompson et al., 2013). Xie et al. (2002) reported the coexistence of tuite and Na-hollandite [$NaAlSi_3O_8$] in the shock-produced veins of the Suizhou chondrite. Natural K-hollandite may exist as a solid-solution phase containing $NaAlSi_3O_8$ (Yagi et al., 1994). Thus, we consider tuite and/or K-hollandite to be essential phases in the mantle source of Baekdusan magmatism.

Low-Si melts and some high-Si melts exhibit a slight negative anomaly in Nb-Ta relative to the neighboring La (Fig. 4c and d). This apparent anomaly could be accounted for by crustal contamination during magma differentiation, because continental crust has a distinct negative Nb-Ta anomaly (e.g., Rudnick and Gao, 2005). We note, however, that $(Nb/La)_N$ ratios do not show a meaningful correlation with the Fo values of host olivines (Fig. 7a), implying an insignificant role for AFC (assimilation and fractional crystallization) processes. This has also been substantiated by previous studies (e.g., Kuritani et al., 2011; Liu et al., 2015a), which found no discernible correlations between SiO_2 and $^{87}Sr/^{86}Sr$ or Ba/Th ratios in the Baekdusan basalts. Instead, we observe a meaningful negative correlation between $(Nb/La)_N$ and $(P/P^*)_N$ ratios (Fig. 7b), where $(P^*)_N = (Nd_N + Sm_N)/2$. The partition coefficient (D) of La between apatite and basaltic melt is significantly higher than that of Nb (D_{La}=1.9–13.3, D_{Nb} = 0.0011–0.0035, D_{Ta} = 0.0010–0.0026; Prowatke and Klemme, 2006). Thus, inasmuch as partitioning coefficients for tuite are unknown, we suggest that the

Nb-Ta depletion might be attributed to relative enrichment in La by presence of tuite in the source.

The magmatism at Baekdusan is characterized by positively fractionated $(Zr/Hf)_N$ ratios, in contrast to OIB (Fig. 4c and d). Recycled oceanic crust (e.g., eclogite or garnet pyroxenite) has been proposed as a reservoir with a suprachondritic Zr/Hf ratio (Klemme et al., 2002; Pertermann et al., 2004). Experimental studies (Hauri et al., 1994; Pertermann et al., 2004; van Westrenen et al., 1999) show complementary D_{Zr} and D_{Hf} values in clinopyroxene ($D_{Zr} < D_{Hf}$) and garnet ($D_{Zr} > D_{Hf}$). The partition coefficient for Zr and Hf in tuite might be about one order of magnitude lower than that determined for clinopyroxene and garnet (Prowatke and Klemme, 2006). The Zr/Hf ratio in melt can thus be controlled by the modal proportions of clinopyroxene and garnet in the source. Fig. 8a shows the Zr/Hf versus La/Yb relationship in partial melts derived from eclogite and peridotite, calculated using the Shaw's (1970) equation. The peridotite is assumed to melt non-modally, but the eclogite in modal proportions. The partition coefficients between minerals and melts, and the concentrations of select trace elements used in the calculations are listed in Table S6. Notably, partial melting of garnet peridotite alone is unlikely to produce the elevated Zr/Hf ratios observed in the Baekdusan melts. The Baekdusan data are best approximated by admixture of partial melts derived from clinopyroxene-rich eclogite and garnet peridotite (Fig. 8a).

To examine the relative contributions of garnet- or spinel-facies sources, we calculated Dy/Yb ratios and Yb concentrations for melts (Fig. 8b). Garnet preferentially incorporates heavy rare earth elements over LREE relative to spinel (McKenzie and O'Nions, 1991; Pertermann et al., 2004). Therefore, garnet peridotite produces a melt with a higher Dy/Yb ratio and lower Yb content than a spinel peridotite source (Fig. 8b). Partial melts derived from spinel-garnet peridotite contain slightly elevated Yb and a reduced Dy/Yb compared with those of garnet peridotite (Fig. 8b). The Baekdusan melts have Dy/Yb ratios

overlapping with those of partial melts from a garnet peridotite, but their Yb contents are too high for modeled melts of garnet peridotite (Fig. 8b). Clinopyroxene-rich eclogites can produce melts with Yb contents higher than a garnet peridotite source (Fig. 8b), which further supports a mixed garnet peridotite-eclogite source.

The sub-alkaline group exhibits lower abundances of incompatible trace elements than the high-Si alkaline group (Fig. 4a, c). Meanwhile, both groups show similar geochemical characteristics such as positive anomalies in Eu, Ba, Rb, K, Pb, and P, and positively fractionated $(Zr/Hf)_N$ ratios compared with OIB (Fig. 4a, c), indicating different degrees of partial melting from the same source. The sub-alkaline melts represent a higher degree of partial melting than the alkaline melts (Fig. 8a, b).

In summary, there are at least two distinct source materials (i.e., altered oceanic crust component (tuite-bearing eclogite) and sediment component (metasomatic agent from K-hollandaite) together with a garnet peridotite component for the Baekdusan magmatism. The concentrations of incompatible elements were modeled in order to investigate the nature of the mantle source of Baekdusan magmatism (Fig. 9). The partition coefficient between minerals and melts, and concentrations of trace elements used in the calculations are provided in Table S7. We used an "enriched" depleted MORB source (E-DMM; Workman and Hart, 2005) for modeling. For high-Si melts, we first assumed a metasomatized mantle [a mixture of 0.5% K-hollandite (Rapp et al., 2008) and 99.5% E-DMM], and P-rich melt I [a mixture of 5% tuite melt (Zhai et al., 2014) and 95% of a 1% eclogite melt]. We used two approaches to determine high-Si melt compositions: (1) a 3% partial melt of a hybrid source [95% metasomatized mantle and 5% P-rich melt I] (Model 1), and (2) a mixture containing 90% of a 1% partial melt of metasomatized mantle and 10% P-rich melt I (Model 2). Phase proportions (by weight) in the solid and melt modes for the metasomatized mantle are $Ol_{55}Opx_{25}Cpx_{10}Grt_{10}$ and $Ol_5Opx_5Cpx_{45}Grt_{45}$, respectively, whereas those for eclogite are the

same as $Cpx_{89}Grt_{11}$. Eclogite compositions were determined using the average oceanic crust values from the PetDB database and the mobility of elements during slab dehydration (Becker et al., 2000; Kogiso et al., 1997). Model 1 is strongly enriched in large-ion lithophile elements (LILE) and exhibits positive anomalies in Pb and P, but no meaningful anomaly in K (Fig. 9a). On the other hand, Model 2 has characteristic spikes in K along with Pb and P, and a positive $(Zr/Hf)_N$ ratio, as observed in high-Si melts (Fig. 9a). For the low-Si group, we assumed P-rich melt II [a mixture of 7% tuite melt and 93% of a 1% eclogite melt], and a hypothetical mantle [90% E-DMM with 10% P-rich melt II]. We modeled low-Si melt compositions in two ways: (1) a 2% partial melt of a hypothetical mantle (Model 3), and (2) 75% of a 1% melt of E-DMM with 25% P-rich melt II (Model 4). Model 3 yield melt compositions significant enriched in LILEs compared with low-Si melts (Fig. 9b). Also note that Model 3 has a positive anomaly in Pb, contrary to observations in low-Si melts (Fig. 9b). Meanwhile, the elemental abundances in Model 4 match those of the low-Si melts, exhibiting a positive anomaly in P and negative anomalies in K and Rb (Fig. 9b). Taken together, we suggest that the high-Si melts may have originated from an enriched MORB mantle source together with subordinate amount of K-hollandite and tuite-bearing eclogite, and the low-Si melts came from the same source but with insignificant contribution from K-hollandite.

5.2. Tectonic implications

To account for the mineral phases (K-hollandite, tuite) present in the source, the Baekdusan magmatism must be derived from a mantle source deeper than ~10 GPa. Recently, replacement of thick (~150–220 km), cold, refractory Archean lithospheric mantle by thin (~60–120 km), hot, fertile Cenozoic lithospheric mantle has been reported from the eastern NCC (Gao et al., 2002; Griffin et al., 1998; Menzies et al., 1993; Menzies and Xu, 1998; Xu, 2001; Yang et al., 2010). Dramatic changes in the mechanical, thermal, and chemical

characteristics of the lithospheric mantle may record the removal of Archean lithospheric mantle during the Phanerozoic, possibly via delamination (Gao et al., 2002; Menzies et al., 1993; Menzies and Xu, 1998). Removal of thickened lower continental crust comprising eclogitic rocks may be accompanied by lithospheric mantle delamination (Gao et al., 2004, 2008). Lower crustal materials foundered in the convecting mantle could provide a mafic source for Baekdusan's magmatism. However, it is still unclear whether the delaminated lower crust reaches a depth near the upper boundary of the subducted Pacific plate, and its duration in the asthenospheric mantle is also unknown. It should be noted that melts derived from foundered eclogitic lower continental crust are characterized by strong depletion of HFSEs, a highly radiogenic initial $^{87}Sr/^{86}Sr$ ratio (0.7053 to 0.7101), and negative ε_{Nd} values (−14 to +2) (e.g., Gao et al., 2004, 2008; Xu et al., 2002, 2006, 2008). As discussed above, the Baekdusan melts do not show any obvious geochemical characteristics of crustal contamination. Furthermore, the Sr-Nd isotopic compositions of the Baekdusan basaltic rocks are generally close to bulk silicate Earth values ($^{87}Sr/^{86}Sr$ = 0.7046 to 0.7062; ε_{Nd} = −4 to +3; Basu et al., 1991; Kuritani et al., 2009; Liu et al., 2015a; Zhang et al., 2015). We thus rule out the possibility of foundered lower continental crustal materials in the source.

Instead, we propose recycled oceanic crust as a possible source of eclogitic materials. Oceanic crust may have been recycled into the mantle beneath northeastern China in dual subduction episodes: (1) the southward subduction of the Mongol-Okhotsk oceanic plate until the Jurassic (Tang et al., 2014; Zhang et al., 2016; Zhou et al., 2009) and (2) the northwestward subduction of the Pacific plate since the Cretaceous (Duan et al., 2009; Guo et al., 2016; Huang and Zhao, 2006; Lei and Zhao, 2005; Liu et al., 2015b; Zhao et al., 2009). Subduction of the Mongol-Okhotsk oceanic plate ceased about 150 Ma ago, and the subducted slab penetrated down to the lower mantle (from depths of ~1,500 km to at least 2,500 km) (van der Voo et al., 1999). No high-velocity seismic anomalies, which would

signify the presence of slab remnants from the Mongol-Okhotsk oceanic plate, have been detected in the upper mantle beneath northeastern China (e.g. Huang and Zhao, 2006; Wei et al., 2012). Intraplate volcanism in northeastern Asia is thus considered to be closely associated with deep subduction of the Pacific plate (e.g., Lei and Zhao, 2005; Tang et al., 2014; Tian et al., 2016; Wei et al., 2012, 2015; Zhao et al., 2009). Seismic tomography of northeastern Asia has revealed a prominent low-velocity anomaly beneath the Baekdusan volcano, extending down to the 410-km discontinuity (Duan et al., 2009; Guo et al., 2016; Huang and Zhao, 2006; Lei et al., 2013; Lei and Zhao, 2005; Tian et al., 2016; Zhao et al., 2009), which may indicate a wet plume from the mantle transition zone (MTZ) (Kuritani et al., 2011; Richard and Iwamori, 2010; Zhao et al., 2009).

Continent-derived sediments subducted along with the oceanic lithosphere can be stored in the MTZ. K-hollandite may be the most dominant phase within stagnant subducted continent-derived sediments, and is also a major repository of LILEs (e.g., K, Ba, Sr, Pb, LREE, etc.) (Irifune et al., 1994; Murphy et al., 2002; Ono, 1998; Rapp et al., 2008). The thermal stability of K-hollandite is dependent upon the amount of H_2O in the system (Rapp et al., 2008); it decomposes around 1600°C at 16 GPa under relatively dry conditions, but breaks down at ~1400°C under wet conditions (Rapp et al., 2008; Wang and Takahashi, 1999). Subducting sediments can carry H_2O to the mantle transition zone (Kerrick and Connolly, 2001a; Ono, 1998). The H_2O fluid released from the subducting slab migrates into the overlying mantle peridotite, and can be trapped to form hydrous phases in peridotites or even incorporated into nominally anhydrous minerals (e.g., wadsleyite, ringwoodite) (Iwamori, 2007; Kawamoto et al 1996; Luth, 2005; Ohtani et al., 2004). Hydrous peridotite is likely to be dragged down by the descending slab, and can also transport H_2O into the transition zone (Ohtani et al., 2004; Ono, 1998). The exact amount of H_2O transported to the transition zone depends on the thermal structure of the subducting slab (Kerrick and Connolly,

2001a, b; Luth, 2005; Ohtani et al., 2004; Ono, 1998). If the subducted stagnant slab and its accompanying peridotite warm to ambient mantle temperatures, thermal decomposition of K-hollandite can occur. Fluids or melts expelled from the breakdown of K-hollandite may facilitate the transfer of LILEs into the mantle above the stagnant slab, where they can metasomatize the ambient mantle peridotite (Kuritani et al., 2011). In addition, the presence of H_2O in peridotite may induce Rayleigh-Taylor instabilities and thus generate wet plumes (Richard and Bercovici, 2009; Richard and Iwamori, 2010), which may pick up stagnant slab materials (Fig. 10). Alternatively, seismic images and waveform modelling show that focused mantle upwelling may rise through a gap in the deep stagnant slabs beneath northeast China (Lei et al., 2013; Tang et al., 2014). Tuite can exist within peridotitic or MORB-like bulk compositions (Konzett et al., 2012) and is stable over a wide range of subduction zone temperature regimes, but not in convecting asthenospheric mantle (Konzett and Frost, 2009; Konzett et al., 2012). When plumes ascend through the upper mantle, metasomatized mantle and recycled oceanic crustal materials (tuite-bearing eclogite or garnet pyroxenite) may undergo partial melting as soon as they surpass the solidus temperature (Fig. 10). The solidus for recycled oceanic crust falls at temperatures ~50 to 150°C lower than that of typical peridotite, and is therefore encountered first during adiabatic upwelling of mantle (Hirschmann and Stolper, 1996; Kogiso et al., 2003). High concentrations of alkali, especially K_2O, in peridotites have a great influence on solidus temperatures, which decrease with increasing alkali content, possibly due to incompatible behavior during partial melting (Herzberg et al., 2000; Hirschmann, 2000). For example, the solidus temperature can decrease by ~150°C per percent alkali in the bulk composition (Herzberg et al., 2000; Hirschmann, 2000). Thus, the difference between the solidus temperatures for LILE-enriched peridotites created by K-hollandite breakdown and recycled oceanic crust may be minor. K-rich melts from metasomatized mantle, P-rich melts from recycled oceanic crust, and

heterogeneous mixtures of these two components may result in compositionally diverse melt inclusions in olivines from the Baekdusan basalts (Fig. 10). We note that the TiO_2 and P_2O_5 contents of the melt inclusions are higher than those of the host basalts (Fig. 3b, g). This observation suggests that there must have been another component having low TiO_2 and P_2O_5 in the host magma, probably produced by prevailing peridotites. The absence of melt inclusions having low TiO_2 and P_2O_5 suggests that the olivine phenocrysts were grown in the mantle source before significant melting of peridotite component. This is consistent with the observation of relatively low Fo values (72-83; Table S3) of the inclusion-bearing olivines.

6. Conclusions

Olivine-hosted melt inclusions in Baekdusan basalts can be divided into two major groups in terms of their major and trace element compositions: a low-Si group and a high-Si group. The low-Si group is characterized by a distinct positive spike for P in the spidergram, as well as a positive correlation between CaO and P_2O_5. The high-Si group exhibits pronounced positive anomalies in Eu, Ba, Rb, K, Pb, and P. They are characterized by fractionated $(Zr/Hf)_N$ ratios higher than the OIB. Geochemical modeling indicates that the high-Si melts may be produced by mixing K-rich melt from the "enriched" depleted MORB source (E-DMM) metasomatized by K-hollandite breakdown with P-rich melt from tuite-bearing eclogite. Meanwhile, the low-Si melts may have been formed by admixture of a melt from E-DMM with a P-rich melt from tuite-bearing eclogite. Partial melting of recycled oceanic crustal materials entrained within a plume ascending from the mantle transition zone or from depths near 700 km through a gap in the stagnant slab along with garnet peridotites may have played an important role in the genesis of volcanism at Baekdusan.

Acknowledgements

This work was funded by the Korea Meteorological Administration Research and Development Program under Grant KMIPA2015-7090. We would like to thank to Nadja Omara Cintron Franqui for her help during the experimental work. Insightful reviews by Takeshi Kuritani and an anonymous reviewer greatly improved the manuscript. We thank Sun-Lin Chung for the editorial handling.

References

Basu, A.R., Wang, J., Huang, W., Xie, G., Tatsumoto, M., 1991. Major element, REE, and Pb, Nd and Sr isotopic geochemistry of Cenozoic volcanic rocks of eastern China: implications for their origin from suboceanic-type mantle reservoirs. Earth and Planetary Science Letters 105, 149–169.

Becker, H., Jochum, K.P., Carlson, R.W., 2000. Trace element fractionation during dehydration of eclogites from high-pressure terranes and the implications for element fluxes in subduction zones. Chemical Geology 163, 65–99.

Chen, J., Hsu, C., Ho, K., 2003. Geochemistry of Cenozoic volcanic rocks and related ultramafic xenoliths from the Jilin and Heilongjiang provinces, northeast China. Journal of Asian Earth Science 21, 1069–1084.

Chen, Y., Provost, A., Schiano, P., Cluzel, N., 2011. The rate of water loss from olivine-hosted melt inclusions. Contributions to Mineralogy and Petrology 162, 625–636.

Chen, Y., Zhang, Y., Graham, D., Su, S., Deng, J., 2007. Geochemistry of Cenozoic basalts and mantle xenoliths in Northeast China. Lithos 96, 108–126.

Cherniak, D.J., 2010. REE diffusion in olivine. American Mineralogist 95, 362–368.

Choi, S.H., Schiano, P., Chen, Y., Devidal, J.-L., Choo, M.K., Lee, J.-I., 2013. Melt inclusions in olivine and plagioclase phenocrysts from Antarctic–Phoenix Ridge basalts: Implications for origins of N- and E-type MORB parent magmas. Journal of Volcanology and Geothermal Research 253, 75–86.

Chu, Z.-Y., Harvey, J., Liu, C.-Z., Guo, J.-H., Wu, F.-Y., Tian, W., Zhang, Y.-L., Yang, Y.-H., 2013. Source of highly potassic basalts in northeast China: Evidence from Re–Os, Sr–Nd–Hf isotopes and PGE geochemistry. Chemical Geology 357, 52–66.

Cottrell, E., Spiegelman, M., Langmuir, C.H., 2002. Consequences of diffusive reequilibration for the interpretation of melt inclusions. Geochemistry Geophysics Geosystem 3, 1–26.

Cui, Z., Wei, H., Liu, R., 1995. A textual research on the historic records of the eruptions from Tianchi Volcano, Changbaishan. in: Connection of Volcanism and Human Environment. Seismic Press, pp. 36–39.

Danyushevsky, L.V., Della-Pasqua, F.N., Sokolov, S., 2000. Re-equilibration of melt inclusions trapped by magnesian olivine phenocrysts from subduction-related magmas: petrological implications. Contributions to Mineralogy and Petrology 138, 68–83.

Danyushevsky, L.V., McNeill, A.W., Sobolev, A.V., 2002. Experimental and petrological studies of melt inclusions in phenocrysts from mantle-derived magmas: an overview of techniques, advantages and complications. Chemical Geology 183, 5–24.

Danyushevsky, L.V., Plechov, P., 2011. Petrolog3: Integrated software for modeling crystallization processes. Geochemistry Geophysics Geosystem 12, Q07021.

Duan, Y., Zhao, D., Zhang, X., Xia, S., Liu, Z., Wang, F., Li, L., 2009. Seismic structure and origin of active intraplate volcanoes in Northeast Asia. Tectonophysics 470, 257–266.

Eisele, J., Sharma, M., Galer, S.J.G., Blichert-Toft, J., Devey, C.W., Hofmann, A.W., 2002. The role of sediment recycling in EM-1 inferred from Os, Pb, Hf, Nd, Sr isotope and

trace element systematics of the Pitcairn hotspot. Earth and Planetary Science Letters 196, 197–212.

Eizenhöfer, P.R., Zhao, G., Zhang, J., Sun, M., 2014. Final closure of the Paleo-Asian Ocean along the Solonker Suture Zone: Constraints from geochronological and geochemical data of Permian volcanic and sedimentary rocks. Tectonics 33, 441–463.

Fan, Q.C., Sui, J.L., Wang, T.H., Li, N., Sun, Q., 2006. Eruption history and magma evolution of the trachybasalt in the Tianchi volcano, Changbaishan. Acta Petrologica Sinica 22, 1449–1457 (in Chinese with English abstract).

Fan, Q.C., Sui, J.L., Wang, T.H., Li, N., Sun, Q., 2007. History of volcanic activity, magma evolution and eruptive mechanisms of the Changbai Volcanic Province. Geological Journal of China Universities 13, 175–190 (in Chinese with English abstract).

Gaetani, G.A., Watson, E.B., 2000. Open system behavior of olivine-hosted melt inclusions. Earth and Planetary Science Letters 183, 27–41.

Gao, S., Rudnick, R.L., Carlson, R.W., McDonough, W.F., Liu, Y.-S., 2002. Re–Os evidence for replacement of ancient mantle lithosphere beneath the North China craton. Earth and Planetary Science Letters 198, 307–322.

Gao, S., Rudnick, R.L., Xu, W.-L., Yuan, H.-L., Liu, Y.-S., Walker, R.J., Puchtel, I.S., Liu, X., Huang, H., Wang, X.-R., Yang, J., 2008. Recycling deep cratonic lithosphere and generation of intraplate magmatism in the North China Craton, Earth and Planetary Science Letters 270, 41–53.

Gao, S., Rudnick, R.L., Yuan, H.-L., Liu, X.-M., Liu, Y.-S., Xu, W.-L., Ling, W.-L., Ayers, J., Wang, X.-C., Wang, Q.-H., 2004. Recycling lower continental crust in the North China craton. Nature 432, 892–897.

Griffin, W.L., Andi, Z., O'Reilly, S.Y., Ryan, C.G., 1998. Phanerozoic Evolution of the Lithosphere Beneath the Sino-Korean Craton, in: Mantle Dynamics and Plate Interactions in East Asia. American Geophysical Union, pp. 107–126.

Guo, W.F., Liu, J.Q., Guo, Z.F., 2014. Temporal variations and petrogenetic implications in Changbai basaltic rocks since the Pliocene. Acta Petrologica Sinica 30, 3595–3611 (in Chinese with English abstract).

Guo, Z., Chen, Y.J., Ning, J., Yang, Y., Afonso, J.C., Tang, Y., 2016. Seismic evidence of on-going sublithosphere upper mantle convection for intra-plate volcanism in Northeast China, Earth and Planetary Science Letters 433, 31–43.

Gurenko, A.A., Chaussidon, M., 1995. Enriched and depleted primitive melts included in olivine from Icelandic tholeiites: origin by continuous melting of a single mantle column. Geochimica et Cosmochimica Acta 59, 2905–2917.

Hauri, E.H., 1996. Major-element variability in the Hawaiian mantle plume. Nature 382, 415–419.

Hauri, E.H., Wagner, T.P., Grove, T.L., 1994. Experimental and natural partitioning of Th, U, Pb and other trace elements between garnet, clinopyroxene and basaltic melts. Chemical Geology 117, 149–166.

Herzberg, C., 2011. Identification of source lithology in the Hawaiian and Canary Islands: Implications for origins. Journal of Petrology 52, 113–146.

Herzberg, C., Raterron, P., Zhang, J., 2000. New experimental observations on the anhydrous solidus for peridotite KLB-1. Geochemistry Geophysics Geosystem 1, 2000GC000089.

Hirschmann, M.M., 2000. Mantle solidus: experimental constraints and the effects of peridotite composition. Geochemistry Geophysics Geosystem 1, 2000GC000070.

Hirschmann, M.M., Kogiso, T., Baker, M.B., Stolper, E.M., 2003. Alkalic magmas generated by partial melting of garnet pyroxenite. Geology 31, 481–484.

Hirschmann, M.M., Stolper, E.M., 1996. A possible role for garnet pyroxenite in the origin of the "garnet signature" in MORB. Contributions to Mineralogy and Petrology 124, 185–208.

Hong, L.-B., Zhang, Y.-H., Qian, S.-P., Liu, J.-Q., Ren, Z.-Y., Xu, Y.-G., 2013. Constraints from melt inclusions and their host olivines on the petrogenesis of Oligocene-Early Miocene Xindian basalts, Chifeng area, North China Craton. Contributions to Mineralogy and Petrology 165, 305–326.

Horn, S., Schmincke, H.-U., 2000. Volatile emission during the eruption of Baitoushan Volcano (China/North Korea) ca. 969 AD. Bulletin of Volcanology 61, 537–555.

Hsu, C.-N., Chen, J.-C., Ho, K.-S., 2000. Geochemistry of Cenozoic volcanic rocks from Kirin Province, northeast China. Geochemical Journal 34, 33–58.

Huang, J., Zhao, D., 2006. High-resolution mantle tomography of China and surrounding regions. Journal of Geophysical Research 111, B09305.

Iacovino, K., Kim, J.-S., Sisson, T., Lowenstern, J., Ri, K.-H., Jang, J.-N., Song, K.-H., Ham, S.-H., Oppenheimer, C., Hammond, J.O.S., Donovan, A., Liu, K.W., Ryu, K.-R., 2016. Quantifying gas emissions from the "Millennium Eruption" of Paektu volcano, Democratic People's Republic of Korea/China. Science Advances 2, e1600913.

Irifune, T., Ringwood, A.E., Hibberson, W.O., 1994. Subduction of continental crust and terrigenous and pelagic sediments: an experimental study. Earth and Planetary Science Letters 126, 351–368.

Irvine, T.N., Baragar, W.R.A., 1971. A guide to the chemical classification of the common volcanic rocks. Canadian Journal of Earth Sciences 8, 523–548.

Iwamori, H., 2007. Transportation of H_2O beneath the Japan arcs and its implications for global water circulation. Chemical Geology 239, 182–198.

Jarosewich, E., Nelen, J.A., Norberg, J.A., 1979. Electron microprobe reference samples for mineral analyses. Smithsonian contributions to the earth sciences 22, Smithsonian Institution Press. 68–72.

John, T., Scherer, E.E., Haase, K., Schenk, V., 2004. Trace element fractionation during fluid-induced eclogitization in a subducting slab: trace element and Lu–Hf–Sm–Nd isotope systematics. Earth and Planetary Science Letters 227, 441–456.

Kamenetsky, V.S., Eggins, S.M., Crawford, A.J., Green, D.H., Gasparon, M., Falloon, T.J., 1998. Calcic melt inclusions in primitive olivine at 43°N MAR: evidence for melt–rock reaction/melting involving clinopyroxene-rich lithologies during MORB generation. Earth and Planetary Science Letters 160, 115–132.

Kawamoto, T., Hervig, R.L., Holloway, J.R., 1996. Experimental evidence for a hydrous transition zone in the early Earth's mantle. Earth and Planetary Science Letters 142, 587–592.

Kendrick, M.A., Jackson, M.G., Kent, A.J.R., Hauri, E.H., Wallace, P.J., Woodhead, J., 2014. Contrasting behaviours of CO_2, S, H_2O and halogens (F, Cl, Br, and I) in enriched-mantle melts from Pitcairn and Society seamounts. Chemical Geology 370, 69–81.

Kent, A.J.R., 2008. Melt inclusions in basaltic and related volcanic rocks. Reviews in Mineralogy and Geochemistry 69, Mineralogical Society of America pp. 273–331.

Kent, A.J.R., Norman, M.D., Hutcheon, I.D., Stolper, E.M., 1999. Assimilation of seawater-derived components in an oceanic volcano: evidence from matrix glasses and glass inclusions from Loihi seamount, Hawaii. Chemical Geology 156, 299–319.

Kerrick, D.M., Connolly, J.A.D., 2001a. Metamorphic devolatilization of subducted marine sediments and the transport of volatiles into the Earth's mantle. Nature 411, 293–296.

Kerrick, D.M., Connolly, J.A.D., 2001b. Metamorphic devolatilization of subducted oceanic metabasalts: implications for seismicity, arc magmatism and volatile recycling. Earth and Planetary Science Letters 189, 19–29.

Keshav, S., Gudfinnsson, G.H., Sen, G., Fei, Y., 2004. High-pressure melting experiments on garnet clinopyroxenite and the alkalic to tholeiitic transition in ocean-island basalts. Earth and Planetary Science Letters 223, 365–379.

Klemme, S., Blundy, J.D., Wood, B.J., 2002. Experimental constraints on major and trace element partitioning during partial melting of eclogite. Geochimica et Cosmochimica Acta 66, 3109–3123.

Kogiso, T., Hirschmann, M.M., 2006. Partial melting experiments of bimineralic eclogite and the role of recycled mafic oceanic crust in the genesis of ocean island basalts, Earth and Planetary Science Letters 249, 188–199.

Kogiso, T., Hirschmann, M.M., Frost, D.J., 2003. High-pressure partial melting of garnet pyroxenite: possible mafic lithologies in the source of ocean island basalts. Earth and Planetary Science Letters 216, 603–617.

Kogiso, T., Tatsumi, Y., Nakano, S., 1997. Trace element transport during dehydration processes in the subducted oceanic crust: 1. Experiments and implications for the origin of ocean island basalts. Earth and Planetary Science Letters 148, 193–205.

Konzett, J., Frost, D.J., 2009. The high P–T stability of hydroxyl-apatite in natural and simplified MORB—an experimental study to 15 GPa with implications for transport and storage of phosphorus and halogens in subduction zones. Journal of Petrology 50, 2043–2062.

Konzett, J., Rhede, D., Frost, D.J., 2012. The high PT stability of apatite and Cl partitioning between apatite and hydrous potassic phases in peridotite: an experimental study to 19

GPa with implications for the transport of P, Cl and K in the upper mantle. Contributions to Mineralogy and Petrology 163, 277–296.

Kuritani, T., Kimura, J.-I., Miyamoto, T., Wei, H., Shimano, T., Maeno, F., Jin, X., Taniguchi, H., 2009. Intraplate magmatism related to deceleration of upwelling asthenospheric mantle: Implications from the Changbaishan shield basalts, northeast China. Lithos 112, 247–258.

Kuritani, T., Kimura, J.-I., Ohtani, E., Miyamoto, H., Furuyama, K., 2013. Transition zone origin of potassic basalts from Wudalianchi volcano, northeast China. Lithos 156–159, 1–12.

Kuritani, T., Ohtani, E., Kimura, J.-I., 2011. Intensive hydration of the mantle transition zone beneath China caused by ancient slab stagnation. Nature Geoscience 4, 713–716.

Le Maitre, R.W., Bateman, P., Dudek, A., Kelle,r J., Lameyre Le Bas, M.J., Sabine, P.A., Schmid, R., Sorensen, H., Streckeisen, A., Woolley, A.R., Zanettin, B., 1989. A classification of igneous rocks and glossary of terms. Blackwell, Oxford.

Lei, J., Xie, F., Fan, Q., Santosh, M., 2013. Seismic imaging of the deep structure under the Chinese volcanoes: An overview. Physics of the Earth and Planetary Interiors 224, 104–123.

Lei, J., Zhao, D., 2005. P-wave tomography and origin of the Changbai intraplate volcano in Northeast Asia. Tectonophysics 397, 281–295.

Li, H.-Y., Huang, X.-L., Guo, H., 2014. Geochemistry of Cenozoic basalts from the Bohai Bay Basin: implications for a heterogeneous mantle source and lithospheric evolution beneath the eastern North China Craton. Lithos 196, 54–66.

Li, H.-Y., Xu, Y.-G., Ryan, J.G., Huang, X.-L., Ren, Z.-Y., Guo, H., Ning, Z.-G., 2016. Olivine and melt inclusion chemical constraints on the source of intracontinental basalts

from the eastern North China Craton: discrimination of contributions from the subducted Pacific slab. Geochimica et Cosmochimica Acta 178, 1–19.

Liu, D.Y., Nutman, A.P., Compston, W., Wu, J.S., Shen, Q.H., 1992. Remnants of ≥3800 Ma crust in the Chinese part of the Sino-Korean craton. Geology 20, 339–342.

Liu, J., Chen, S., Guo, Z., Guo, W., He, H., You, H., Kim, H., Sung, G., Kim, H., 2015a. Geological background and geodynamic mechanism of Mt. Changbai volcanoes on the China–Korea border. Lithos 236-237, 46–73.

Liu, Y., Gao, S., Kelemen, P.B., Xu, W., 2008. Recycled crust controls contrasting source compositions of Mesozoic and Cenozoic basalts in the North China Craton. Geochimica et Cosmochimica Acta 72, 2349–2376.

Liu, Z., Niu, F., Chen, Y.J., Grand, S., Kawakatsu, H., Ning, J., Tanaka, S., Obayashi, M., Ni, J., 2015b. Receiver function images of the mantle transition zone beneath NE China: new constraints on intraplate volcanism, deep subduction and their potential link, Earth and Planetary Science Letters 412, 101–111.

Lowenstern, J.B., 1995. Applications of silicate-melt inclusions to the study of magmatic volatiles. in: Thompson, J.F.H. (Eds.), Magmas, Fluids, and Ore Deposits. Mineralogical Association of Canada Short Course 23, 71–99.

Luth, R.W., 2005. Mantle volatiles-distribution and consequences. in: Carlson, R.W., Holland, H.D., Turekian, K.K. (Eds.), The Mantle and Core, Treatise on geochemistry 2. Elsevier, pp. 319–361.

Machida, H., Arai, F., 1983. Extensive ash falls in and around the Sea of Japan from large late quaternary eruptions. Journal of Volcanology and Geothermal Research 18, 151–164.

Mathez, E.A., 1976. Sulfur solubility and magmatic sulfides in submarine basalt glass. Journal of Geophysical Research 81, 4269–4276.

McKenzie, D., O'Nions, R.K., 1991. Partial melt distributions from inversion of rare earth element concentrations. Journal of Petrology 32, 1021–1091.

Meng, E., Xu, W.-L., Pei, F.-P., Yang, D.-B., Yu, Y., Zhang, X.-Z., 2010. Detrital-zircon geochronology of Late Paleozoic sedimentary rocks in eastern Heilongjiang Province, NE China: implications for the tectonic evolution of the eastern segment of the Central Asian Orogenic Belt. Tectonophysics 485, 42–51.

Meng, Q.R., 2003. What drove late Mesozoic extension of the northern China–Mongolia tract? Tectonophysics 369, 155–174.

Menzies, M.A., Fan, W., Zhang, M., 1993. Palaeozoic and Cenozoic lithoprobes and the loss of >120 km of Archaean lithosphere, Sino-Korean craton, China, in: Prichard, H.M., Alabaster, T., Harris, N.B.W., Neary, C.R. (Eds.), Magmatic Processes and Plate Tectonics. Geological Society Special Publications 76, 71–81.

Menzies, M.A., Xu, Y., 1998. Geodynamics of the North China Craton, in: Flower, M.F.J., Chung, S.-L., Lo, C.-H., Lee, T.-Y. (Eds.), Mantle Dynamics and Plate Interactions in East Asia, American Geophysical Union, Washington, D.C.

Murayama, J.K., Nakai, S., Kato, M., Kumazawa, M., 1986. A dense polymorph of $Ca_3(PO_4)_2$: a high pressure phase of apatite decomposition and its geochemical significance. Physics of the Earth and Planetary Interiors 44, 293–303.

Murphy, D.T., Collerson, K.D., Kamber, B.S., 2002. Lamproites from Gaussberg, Antarctica: possible transition zone melts of Archaean subducted sediments. Journal of Petrology 43, 981–1001.

Nielsen, R.L., Michael, P.J., Sours-Page, R., 1998. Chemical and physical indicators of compromised melt inclusions. Geochimica et Cosmochimica Acta 62, 831–839.

Ohtani, E., Litasov, K., Hosoya, T., Kubo, T., Kondo, T., 2004. Water transport into the deep mantle and formation of a hydrous transition zone. Physics of the Earth and Planetary Interiors 143–144, 255–269.

Ono, S., 1998. Stability limits of hydrous minerals in sediment and mid-ocean ridge basalt compositions: implications for water transport in subduction zones. Journal of Geophysical Research 103, 18253–18267.

Pertermann, M., Hirschmann, M.M., 2003a. Anhydrous partial melting experiments on MORB-like eclogite: phase relations, phase compositions and mineral–melt partitioning of major elements at 2–3 GPa. Journal of Petrology 44, 2173–2201.

Pertermann, M., Hirschmann, M.M., 2003b. Partial melting experiments on a MORB-like pyroxenite between 2 and 3 GPa: Constraints on the presence of pyroxenite in basalt source regions from solidus location and melting rate. Journal of Geophysical Research 108, 2125.

Pertermann, M., Hirschmann, M.M., Hametner, K., Günther, D., Schmidt, M.W., 2004. Experimental determination of trace element partitioning between garnet and silica-rich liquid during anhydrous partial melting of MORB-like eclogite. Geochemistry Geophysics Geosystem 5, Q05A01.

Prowatke, S., Klemme, S., 2006. Trace element partitioning between apatite and silicate melts. Geochimica et Cosmochimica Acta 70, 4513–4527.

Qian, S.-P., Ren, Z.-Y., Zhang, L., Hong, L.-B., Liu, J.-Q., 2015. Chemical and Pb isotope composition of olivine-hosted melt inclusions from the Hannuoba basalts, North China Craton: implications for petrogenesis and mantle source. Chemical Geology 401, 111–125.

Qin, Z., Lu, F., Anderson, A.T., 1992. Diffuse reequilibration of melt and fluid inclusions. American Mineralogist 77, 565–576.

Ramos, F.C., Heizler, M.T., Buettner, J.E., Gill, J.B., Wei, H.Q., Dimond, C.A., Scott, S.R., 2016. U-series and $^{40}Ar/^{39}Ar$ ages of Holocene volcanic rocks at Changbaishan volcano, China. Geology 44, 511–514.

Rapp, R.P., Irifune, T., Shimizu, N., Nishiyama, N., Norman, M.D., Inoue, T., 2008. Subduction recycling of continental sediments and the origin of geochemically enriched reservoirs in the deep mantle. Earth and Planetary Science Letters 271, 14–23.

Rehkämper, M., Hofmann, A.W., 1997. Recycled ocean crust and sediment in Indian Ocean MORB. Earth and Planetary Science Letters 147, 93–106.

Reid, M.R., 2005. Timescales of magma transfer and storage in the crust. in: Rudnick R.L. (Eds.) The Crust, Treatise on Geochemistry 3, Elsevier, pp 167–193.

Richard, G.C., Bercovici, D., 2009. Water-induced convection in the Earth's mantle transition zone. Journal of Geophysical Research 114, B01205.

Richard, G.C., Iwamori, H., 2010. Stagnant slab, wet plumes and Cenozoic volcanism in East Asia. Physics of the Earth and Planetary Interiors 183, 280–287.

Roedder, E., 1984. Fluid Inclusions, Review in Mineralogy 12, Mineralogical Society of America 646 pp.

Roeder, P.L., Emslie, R.F., 1970. Olivine-liquid equilibrium. Contributions to Mineralogy and Petrology 29, 275–289.

Rudnick, R.L., Gao, S., 2005. Composition of the continental crust. in: Rudnick, R.L. (Eds.), The Crust, Treatise on Geochemistry 3 Elsevier, pp. 1–64.

Sakuyama, T., Tian, W., Kimura, J.-I., Fukao, Y., Hirahara, Y., Takahashi, T., Senda, R., Chang, Q., Miyazaki, T., Obayashi, M., Kawabata, H., Tatsumi, Y., 2013. Melting of dehydrated oceanic crust from the stagnant slab and of the hydrated mantle transition zone: constraints from Cenozoic alkaline basalts in eastern China. Chemical Geology 359, 32–48.

Schiano, P., 2003. Primitive mantle magmas recorded as silicate melt inclusions in igneous minerals. Earth-Science Reviews 63, 121–144.

Schmidt, M.W., 1996. Experimental constraints on recycling of potassium from subducted oceanic crust. Science 272, 1927–1930.

Shaw, D.M., 1970. Trace element fractionation during anatexis, Geochimica et Cosmochimica Acta 34, 237–243.

Shimizu, N., 1998. The geochemistry of olivine-hosted melt inclusions in a FAMOUS basalt ALV519-4-1. Physics of the Earth and Planetary Interiors. 107, 183–201.

Sobolev, A.V, 1996. Melt inclusions in minerals as a source of principle petrological information. Petrology 4, 209–220.

Sobolev, A.V., Danyushevsky, L.V., 1994. Petrology and geochemistry of boninites from the North Termination of the Tonga Trench: constraints on the generation conditions of primary High-Ca boninite magmas. Journal of Petrology 35, 1183–1211.

Sobolev, A.V., Dmitriev, L.V., Barsukov, V.L., Nevsorov, V.N., Slutskii, A.B., 1980. The formation conditions of the high-magnesium olivines from the monomineralic fraction of Luna 24 regolith, in: Lunar and Planetary Science Conference Proceedings, Pergamon Press, New York, USA, pp. 105–116.

Sobolev, A.V., Hofmann, A.W., Kuzmin, D.V., Yaxley, G.M., Arndt, N.T., Chung, S.-L., Danyushevsky, L.V., Elliott, T., Frey, F.A., Garcia, M.O., Gurenko, A.A., Kamenetsky, V.S., Kerr, A.C., Krivolutskaya, N.A., Matvienkov, V.V., Nikogosian, I.K., Rocholl, A., Sigurdsson, I.A., Sushchevskaya, N.M., Teklay, M., 2007. The amount of recycled crust in sources of mantle-derived melts. Science 316, 412–417.

Sobolev, A.V., Hofmann, A.W., Sobolev, S.V., Nikogosian, I.K., 2005. An olivine-free mantle source of Hawaiian shield basalts. Nature 434, 590–597.

Sobolev, A.V., Shimizu, N., 1993. Ultra-depleted primary melt included in an olivine from the Mid-Atlantic Ridge. Nature 363, 151–154.

Spandler, C., O'Neill, H.S.C., Kamenetsky, V.S., 2007. Survival times of anomalous melt inclusions from element diffusion in olivine and chromite. Nature 447, 303–306.

Stolper, E., Sherman, S., Garcia, M., Baker, M., Seaman, C., 2004. Glass in the submarine section of the HSDP2 drill core, Hilo, Hawaii. Geochemistry Geophysics Geosystem 5, Q07G15.

Stone, R., 2011. Vigil at North Korea's Mount Doom. Science 334, 584–588.

Straub, S.M., LaGatta, A.B., Pozzo, A.L.M.-D., Langmuir, C.H., 2008. Evidence from high-Ni olivines for a hybridized peridotite/pyroxenite source for orogenic andesites from the central Mexican Volcanic Belt. Geochemistry Geophysics Geosystem 9, Q03007.

Sugiyama, K., Tokonami, M., 1987. Structure and crystal chemistry of a dense polymorph of tricalcium phosphate $Ca_3(PO_4)_2$: A host to accommodate large lithophile elements in the Earth's mantle. Physics and Chemistry of Minerals. 15, 125–130.

Sun, C., Plunkett, G., Liu, J., Zhao, H., Sigl, M., McConnell, J.R., Pilcher, J.R., Vinther, B., Steffensen, J.P., Hall, V., 2014. Ash from Changbaishan Millennium eruption recorded in Greenland ice: implications for determining the eruption's timing and impact. Geophysical Research Letters 41, 694–701.

Sun, D.-Y., Gou, J., Wang, T.-H., Ren, Y.-S., Liu, Y.-J., Guo, H.-Y., Liu, X.-M., Hu, Z.-C., 2013. Geochronological and geochemical constraints on the Erguna massif basement, NE China – subduction history of the Mongol–Okhotsk oceanic crust. International Geology Review 55, 1801–1816.

Sun, S.-S., McDonough, W.F., 1989. Chemical and isotopic systematics of oceanic basalts: implications for mantle composition and processes. in: Saunders, A.D., Norry, M.J.

(Eds.), Magmatism in the Ocean Basins, Geological Society Special Publication No 42, pp. 313–345.

Tang, J., Obayashi, M., Niu, F., Grand, S.P., Chen, Y.J., Kawakatsu, H., Tanaka, S., Ning, J., Ni, J., 2014. Changbaishan volcanism in northeast China linked to subduction-induced mantle upwelling. Nature Geosciences 7, 470–475.

Tang, J., Xu, W.-L., Wang, F., Wang, W., Xu, M.-J., Zhang, Y.-H., 2014. Geochronology and geochemistry of Early–Middle Triassic magmatism in the Erguna Massif, NE China: Constraints on the tectonic evolution of the Mongol–Okhotsk Ocean. Lithos 184–187, 1–16.

Thompson, R.M., Xie, X., Zhai, S., Downs, R.T., Yang, H., 2013. A comparison of the $Ca_3(PO_4)_2$ and $CaSiO_3$ systems, with a new structure refinement of tuite synthesized at 15 GPa and 1300 °C. American Mineralogist 98, 1585–1592.

Thompson, R.N., Gibson, S.A., 2000. Transient high temperatures in mantle plume heads inferred from magnesian olivines in Phanerozoic picrites. Nature 407, 502–506.

Thornber, C.R., Sherrod, D.R., Siems, D.F., Heliker, C.C., Meeker, G.P., Oscarson, R.L., Kauahikaua, J.P., 2002. Whole-rock and glass major-element geochemistry of Kilauea Volcano, Hawaii, near-vent eruptive products: September 1994 through September 2001 (RPRT), Open-File Report.

Tian, Y., Zhu, H., Zhao, D., Liu, C., Feng, X., Liu, T., Ma, J., 2016. Mantle transition zone structure beneath the Changbai volcano: insight into deep slab dehydration and hot upwelling near the 410 km discontinuity. Journal of Geophysical Research 121, 5794–5808.

Ulmer, P., 1989. The dependence of the Fe^{2+}–Mg cation-partitioning between olivine and basaltic liquid on pressure, temperature and composition. Contributions to Mineralogy and Petrology 101, 261–273.

Urakawa, S., Kondo, T., Igawa, N., Shimomura, O., Ohno, H., 1994. Synchrotron radiation study on the high-pressure and high-temperature phase relations of $KAlSi_3O_8$. Physics and Chemistry of Minerals 21, 387–391.

Van der Voo, R., Spakman, W., Bijwaard, H., 1999. Mesozoic subducted slabs under Siberia. Nature 397, 246–249.

Van Westrenen, W., Blundy, J., Wood, B., 1999. Crystal-chemical controls on trace element partitioning between garnet and anhydrous silicate melt. American Mineralogist 84, 838–847.

Wallace, P., Carmichael, I.S.E., 1992. Sulfur in basaltic magmas. Geochimica et Cosmochimica Acta 56, 1863–1874.

Wang, W., Takahashi, E., 1999. Subsolidus and melting experiments of a K-rich basaltic composition to 27 GPa: Implication for the behavior of potassium in the mantle. American Mineralogist 84, 357–361.

Wang, Y., Li, C., Wei, H., Shan, X., 2003. Late Pliocene–recent tectonic setting for the Tianchi volcanic zone, Changbai Mountains, northeast China. Journal of Asian Earth Science 21, 1159–1170.

Wei, H., Liu, G., Gill, J., 2013. Review of eruptive activity at Tianchi volcano, Changbaishan, northeast China: implications for possible future eruptions. Bulletin of Volcanology 75, 706.

Wei, H., Sparks, R.S.J., Liu, R., Fan, Q., Wang, Y., Hong, H., Zhang, H., Chen, H., Jiang, C., Dong, J., Zheng, Y., Pan, Y., 2003. Three active volcanoes in China and their hazards. Journal of Asian Earth Science 21, 515–526.

Wei, H., Wang, Y., Jin, J., Gao, L., Yun, S.-H., Jin, B., 2007. Timescale and evolution of the intracontinental Tianchi volcanic shield and ignimbrite-forming eruption, Changbaishan, Northeast China. Lithos 96, 315–324.

Wei, W., Xu, J., Zhao, D., Shi, Y., 2012. East Asia mantle tomography: new insight into plate subduction and intraplate volcanism. Journal of Asian Earth Science 60, 88–103.

Wei, W., Zhao, D., Xu, J., Wei, F., Liu, G., 2015. P and S wave tomography and anisotropy in Northwest Pacific and East Asia: constraints on stagnant slab and intraplate volcanism. Journal of Geophysical Research Solid Earth 120, 1642–1666.

Wilkinson, J.F.G., Maitre, R.W.L.E., 1987. Upper mantle amphiboles and micas and TiO_2, K_2O, and P_2O_5 abundances and 100 $Mg/(Mg^{+}Fe^{2+})$ ratios of common basalts and andesites: implications for modal mantle metasomatism and undepleted Mantle compositions. Journal of Petrology 28, 37–73.

Workman, R. K., Hart, S. R., 2005. Major and trace element composition of the depleted MORB mantle (DMM). Earth and Planetary Science Letters 231, 53–72.

Xie, X., Minitti, M.E., Chen, M., Mao, H., Wang, D., Shu, J., Fei, Y., 2002. Natural high-pressure polymorph of merrillite in the shock veins of the Suizhou meteorite. Geochimica et Cosmochimica Acta 66, 2439–2444.

Xu, J.-F., Shinjo, R., Defant, M.J., Wang, Q., Rapp, R.P., 2002. Origin of Mesozoic adakitic intrusive rocks in the Ningzhen area of east China: partial melting of delaminated lower continental crust? Geology 30, 1111–1114.

Xu, J., Liu, G., Wu, J., Ming, Y., Wang, Q., Cui, D., Shangguan, Z., Pan, B., Lin, X., Liu, J., 2012b. Recent unrest of Changbaishan volcano, northeast China: a precursor of a future eruption? Geophysical Research Letters 39, L16305.

Xu, J., Pan, B., Liu, T., Hajdas, I., Zhao, B., Yu, H., Liu, R., Zhao, P., 2013. Climatic impact of the Millennium eruption of Changbaishan volcano in China: new insights from high-precision radiocarbon wiggle-match dating. Geophysical Research Letters 40, 54–59.

Xu, W.-L., Wang, Q.-H., Wang, D.-Y., Guo, J.-H., Pei, F.-P., 2006. Mesozoic adakitic rocks from the Xuzhou-Suzhou area, eastern China: evidence for partial melting of delaminated lower continental crust. Journal of Asian Earth Science 27, 454–464.

Xu, W., Hergt, J.M., Gao, S., Pei, F., Wang, W., Yang, D., 2008. Interaction of adakitic melt-peridotite: implications for the high-Mg# signature of Mesozoic adakitic rocks in the eastern North China Craton, Earth and Planetary Science Letters 265, 123–137.

Xu, Y.-G., 2001. Thermo-tectonic destruction of the Archaean lithospheric keel beneath the Sino-Korean craton in china: evidence, timing and mechanism. Physics and Chemistry of the Earth, Part A: Solid Earth and Geodesy 26, 747–757.

Xu, Y.-G., Ma, J.-L., Frey, F.A., Feigenson, M.D., Liu, J.-F., 2005. Role of lithosphere–asthenosphere interaction in the genesis of Quaternary alkali and tholeiitic basalts from Datong, western North China Craton. Chemical Geology 224, 247–271.

Xu, Y.-G., Zhang, H.-H., Qiu, H.-N., Ge, W.-C., Wu, F.-Y., 2012a. Oceanic crust components in continental basalts from Shuangliao, Northeast China: derived from the mantle transition zone? Chemical Geology 328, 168–184.

Yagi, A., Suzuki, T., Akaogi, M., 1994. High pressure transitions in the system $KAlSi_3O_8$-$NaAlSi_3O_8$. Physics and Chemistry of Minerals 21, 12–17.

Yan, J., Zhao, J.-X., 2008. Cenozoic alkali basalts from Jingpohu, NE China: the role of lithosphere–asthenosphere interaction. Journal of Asian Earth Science 33, 106–121.

Yang, J.-H., O'Reilly, S., Walker, R.J., Griffin, W., Wu, F.-Y., Zhang, M., Pearson, N., 2010. Diachronous decratonization of the Sino-Korean craton: Geochemistry of mantle xenoliths from North Korea. Geology 38, 799–802.

Yaxley, G.M., Green, D.H., 1998. Reactions between eclogite and peridotite: mantle refertilisation by subduction of oceanic crust. Schweizerische Mineralogische und Petrographische Mitteilungen 78, 243–255.

Yi, W., Halliday, A.N., Alt, J.C., Lee, D.-C., Rehkämper, M., Garcia, M.O., Langmuir, C.H., Su, Y., 2000. Cadmium, indium, tin, tellurium, and sulfur in oceanic basalts: Implications for chalcophile element fractionation in the Earth. Journal of Geophysical Research Solid Earth 105, 18927–18948.

Yin, J., Jull, A.J.T., Burr, G.S., Zheng, Y., 2012. A wiggle-match age for the Millennium eruption of Tianchi Volcano at Changbaishan, Northeastern China. Quaternary Science Reviews 47, 150–159.

Yun, S.-H., Koh, J.S., 2014. Petrochemical characteristics of volcanic rocks of historic era at Mt. Baekdusan. Journal of the Geological Society of Korea 50, 753–769 (in Korean with English abstract).

Yun, S.-H., Lee, J.H., 2012. Analysis of unrest signs of activity at the Baegdusan Volcano. Journal of the Petrological Society of Korea 21, 1–12 (in Korean with English abstract).

Zhai, S., Xue, W., Yamazaki, D., Ma, F., 2014. Trace element composition in tuite decomposed from natural apatite in high-pressure and high-temperature experiments. Science China Earth Science 57, 2922–2927.

Zhang, F.-F., Wang, Y.-H., Liu, J.-J., Wang, J.-P., Zhao, C.-B., Song, Z.-W., 2016. Origin of the Wunugetushan porphyry Cu–Mo deposit, Inner Mongolia, NE China: constraints from geology, geochronology, geochemistry, and isotopic compositions. Journal of Asian Earth Science 117, 208–224.

Zhang, J.-J., Zheng, Y.-F., Zhao, Z.-F., 2009. Geochemical evidence for interaction between oceanic crust and lithospheric mantle in the origin of Cenozoic continental basalts in east-central China. Lithos 110, 305–326.

Zhang, M., Guo, Z., 2016. Origin of Late Cenozoic Abaga–Dalinuoer basalts, eastern China: implications for a mixed pyroxenite–peridotite source related with deep subduction of the Pacific slab. Gondwana Research 37, 130–151.

Zhang, M., Guo, Z., Cheng, Z., Zhang, L., Liu, J., 2015. Late Cenozoic intraplate volcanism in Changbai volcanic field, on the border of China and North Korea: insights into deep subduction of the Pacific slab and intraplate volcanism. Journal of the Geological Society 172, 648–663.

Zhang, M., Syddaby, P., Thompson, R.N., Thirlwall, M.F., Menzies, M.A., 1995. Potassic volcanic rocks in NE China: geochemical constraints on mantle source and magma genesis. Journal of Petrology 36, 1275–1303.

Zhang, X., Zhang, Y., Zhai, M., Wu, F., Hou, Q., Yuan, L., 2017. Decoding Neoarchean to Palaeproterozoic tectonothermal events in the Rangnim Massif, North Korea: regional correlation and broader implications. International Geology Review 59, 16–28.

Zhao, D., Tian, Y., Lei, J., Liu, L., Zheng, S., 2009. Seismic image and origin of the Changbai intraplate volcano in East Asia: role of big mantle wedge above the stagnant Pacific slab. Physics of the Earth and Planetary Interiors 173, 197–206.

Zheng, J., Griffin, W.L., O'Reilly, S.Y., Lu, F., Wang, C., Zhang, M., Wang, F., Li, H., 2004. 3.6 Ga lower crust in central China: new evidence on the assembly of the North China craton. Geology 32, 229–232.

Zhou, J.-B., Wilde, S.A., Zhang, X.-Z., Zhao, G.-C., Zheng, C.-Q., Wang, Y.-J., Zhang, X.-H., 2009. The onset of Pacific margin accretion in NE China: evidence from the Heilongjiang high-pressure metamorphic belt. Tectonophysics 478, 230–246.

Zou, H., Fan, Q., Yao, Y., 2008. U–Th systematics of dispersed young volcanoes in NE China: asthenosphere upwelling caused by piling up and upward thickening of stagnant Pacific slab. Chemical Geology 255, 134–142.

Zou, H., Fan, Q., Zhang, H., 2010. Rapid development of the great Millennium eruption of Changbaishan (Tianchi) Volcano, China/North Korea: evidence from U–Th zircon dating. Lithos 119, 289–296.

Zou, H., Fan, Q., Zhang, H., Schmitt, A.K., 2014. U-series zircon age constraints on the plumbing system and magma residence times of the Changbai volcano, China/North Korea border. Lithos 200-201, 169–180.

Figure Captions

Fig. 1. (a) Simplified geological map showing major tectonic units of the North China Craton (NCC) and its surrounding areas, modified from Yan and Zhao (2008). (b) The distribution of Cenozoic volcanic rocks in northeastern China and the location of the study area, after Zhang et al. (2015). (c) Geological map showing fault structures and volcanic distribution in the study area (modified after Wang et al., 2003). Abbreviations: CAOB = Central Asia Orogenic Belt; SH R. = Songhua River; TM R. = Tumen River; YL R. = Yalu River.

Fig. 2. Total alkali versus silica plots (Le Maitre et al., 1989) for corrected melt inclusions in olivines and host basalts. The boundary line dividing alkaline and subalkaline series is from Irvine and Baragar (1971). The gray shaded area represents published data for Baekdusan basaltic rocks (Chen et al., 2007; Fan et al., 2006; Guo et al., 2014; Kuritani et al., 2009; Liu et al., 2015a; Yun and Koh, 2014; Zhang et al., 2015).

Fig. 3. Major oxide patterns of corrected melt inclusions in olivines and host basalts. MI = melt inclusion.

Fig. 4. Rare earth element concentrations normalized to chondrite values (Sun and McDonough, 1989) for corrected melt inclusions and host basalts (a and b), and extended trace element plots normalized to the composition of the primitive mantle (Sun and McDonough, 1989) (c and d). Typical oceanic island basalt (OIB; Sun and McDonough, 1989) compositions are shown for comparison. Solid red circles in (a) and (c) represent the most magnesian melt inclusion (sample BD-07-2). MI = melt inclusion.

Fig. 5. CaO contents versus Fo values of melt inclusion-bearing olivines from Baekdusan basaltic rocks. The dashed line separating magmatic phenocrysts from mantle olivines on the basis of CaO is from Thompson and Gibson (2000).

Fig. 6. P_2O_5 versus CaO contents for corrected melt inclusions and host basalts. MI = melt inclusion.

Fig. 7. Primitive-mantle-normalized $(Nb/La)_N$ ratios for melt inclusions versus (a) Fo values of host olivines and (b) $(P/P^*)_N$ ratios for melt inclusions, where $(P^*)_N = (Nd_N + Sm_N)/2$. Normalization values are from Sun and McDonough (1989). MI = melt inclusion.

Fig 8. (a) Zr/Hf versus La/Yb ratios and (b) Dy/Yb ratio versus Yb (ppm) for melt inclusions from Baekdusan basaltic rocks. Also shown are the melt curves for modal batch melting of eclogites and non-modal batch melting of garnet peridotites, spinel peridotite, and spinel-garnet peridotite using partition coefficients from Table S3. The "enriched"-depleted MORB mantle (E-DMM; Workman and Hart, 2005) and natural eclogite compositions (John et al., 2004) are used for modeling. Phase proportions (by weight) in the solid mode are $Ol_{55}Opx_{20}Cpx_{15}Grt_{10}$ and $Ol_{55}Opx_{25}Cpx_{10}Grt_{10}$ for garnet peridotites, $Ol_{55}Opx_{25}Cpx_{18}Sp_2$ for spinel peridotite, and $Ol_{50}Opx_{25}Cpx_{19}Sp_3Grt_3$ for spinel-garnet peridotite. Phase proportions (by weight) in the melt mode are $Ol_5Opx_5Cpx_{45}Grt_{45}$ for garnet peridotite, $Ol_{10}Opx_{20}Cpx_{68}Sp_2$ for spinel peridotite, and $Ol_7Opx_{10}Cpx_{50}Sp_8Grt_{25}$ for spinel-garnet peridotite. Phase proportions (by weight) for eclogites are $Cpx_{89}Grt_{11}$ and $Cpx_{82}Grt_{18}$, respectively. Abbreviations: Ol = olivine, Opx = orthopyroxene, Cpx = clinopyroxene, Grt = garnet, Sp = spinel, MI = melt inclusion.

Fig. 9. Primitive-mantle-normalized incompatible trace element concentrations of melts modeled using non-modal batch melting (Shaw, 1970) for the high-Si group (a) and the low-Si group (b). See text for details of the modeled melt compositions. Gray lines represent olivine-hosted melt inclusions from Baekdusan basaltic rocks. MI = melt inclusion.

Fig. 10. A schematic illustrating the melting process in the upper mantle beneath Baekdusan.

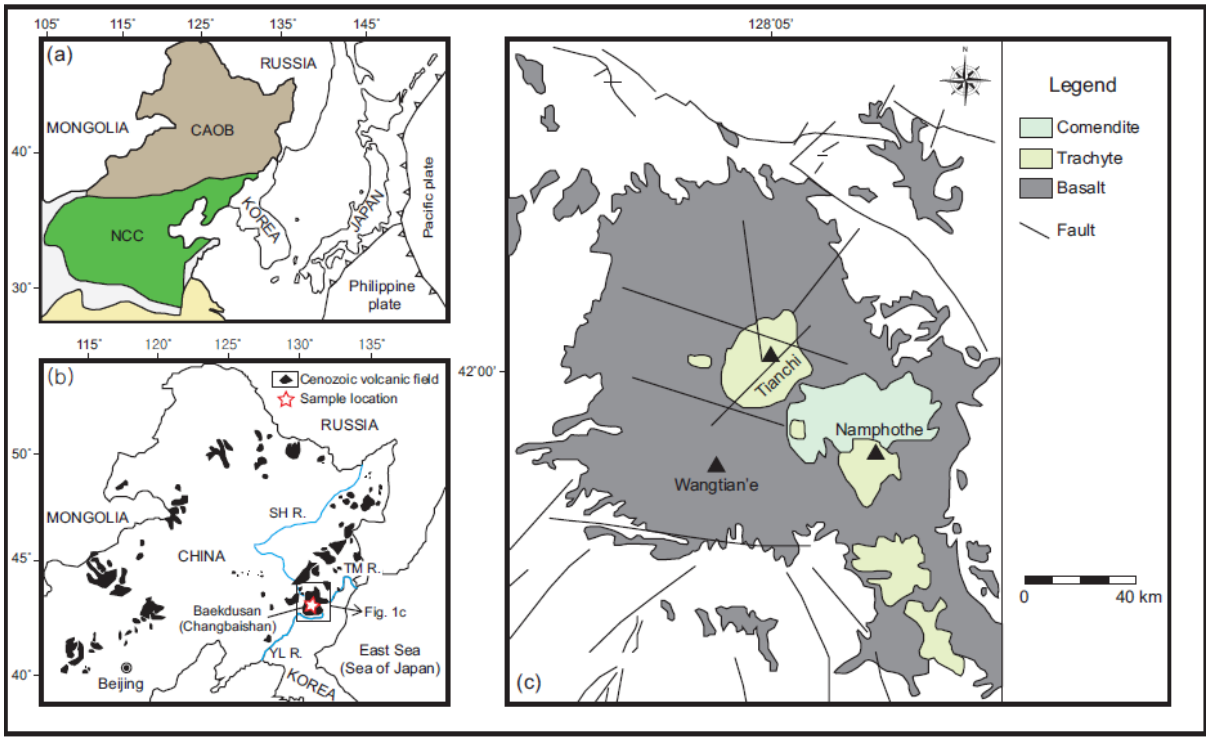

Figure 1

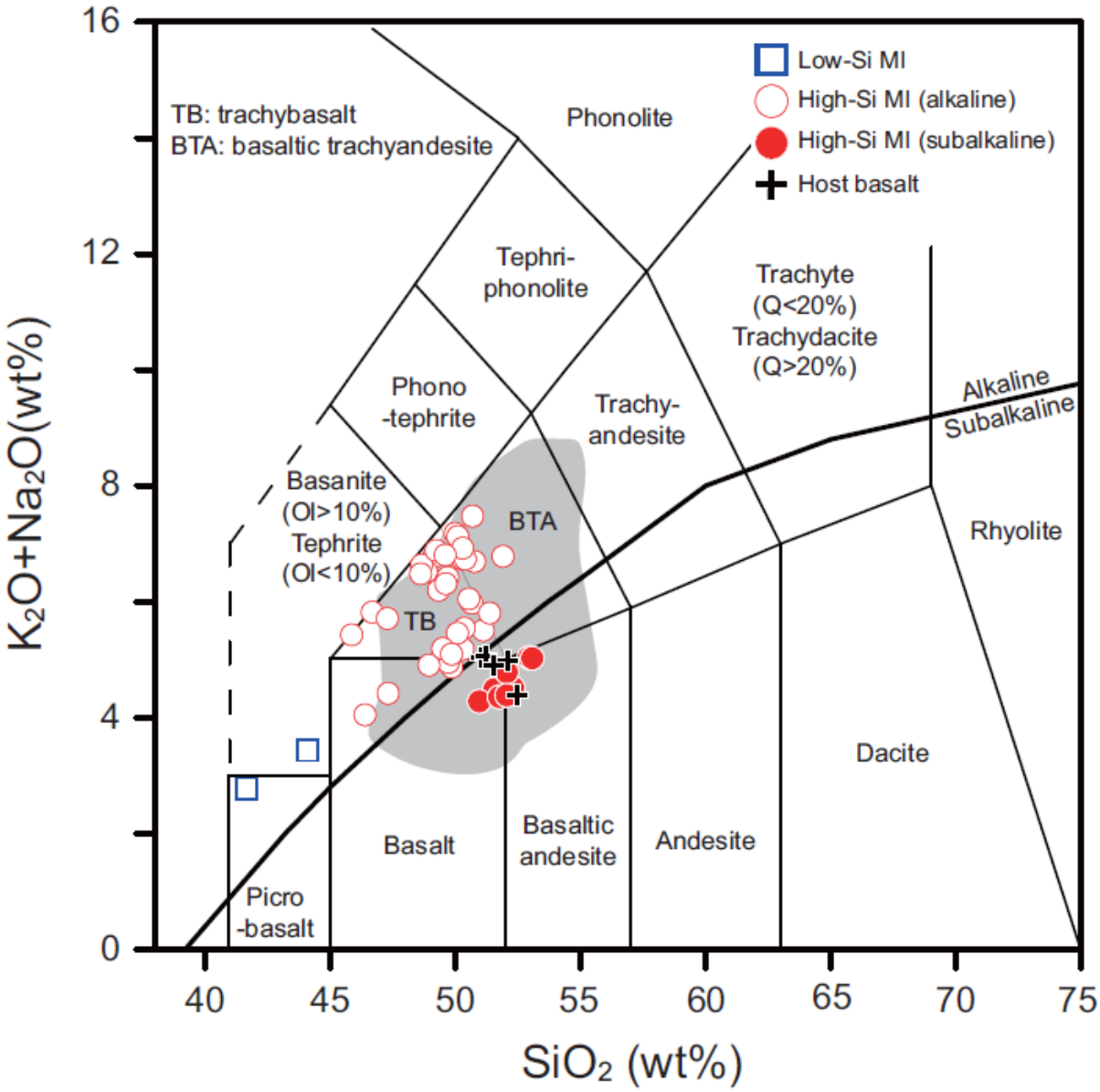

Figure 2

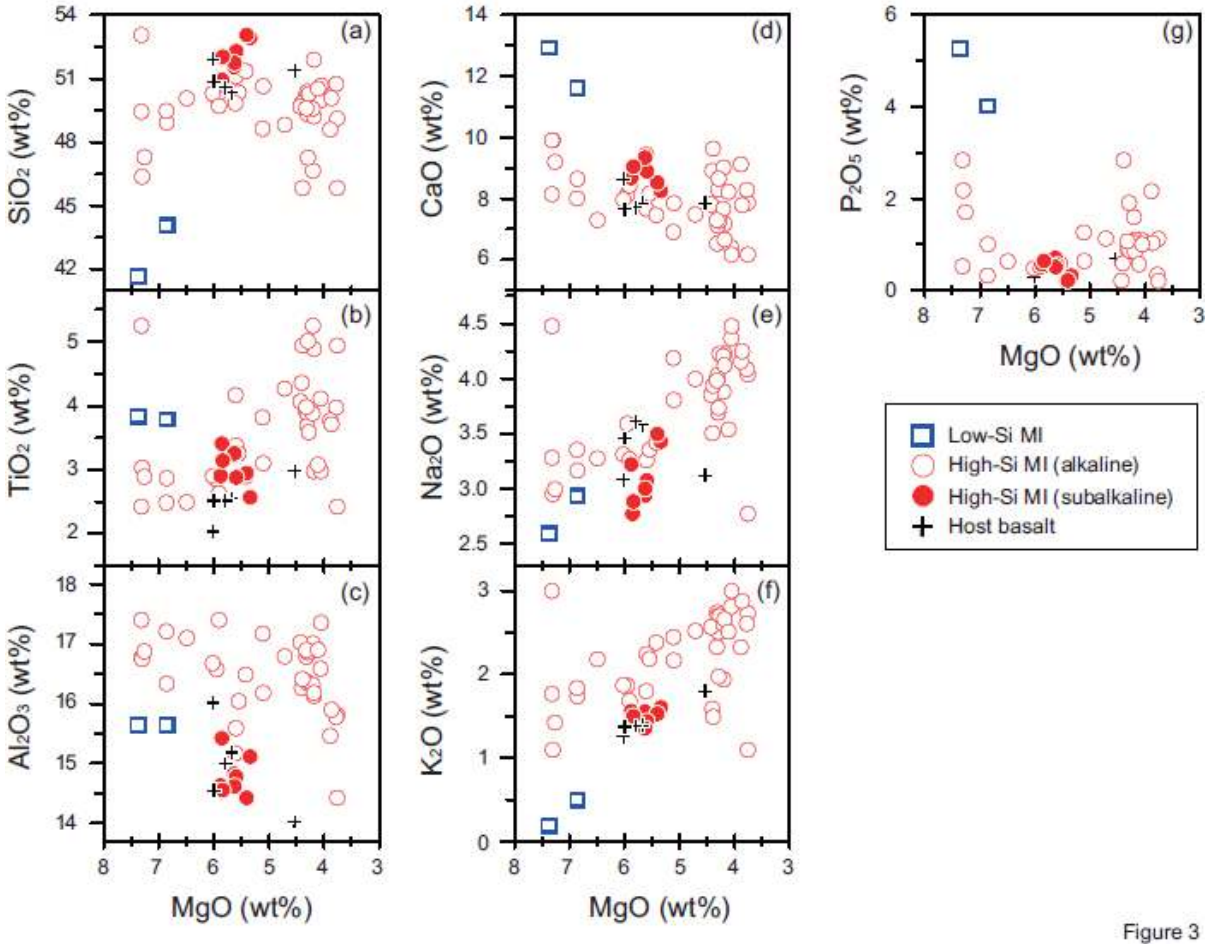

Figure 3

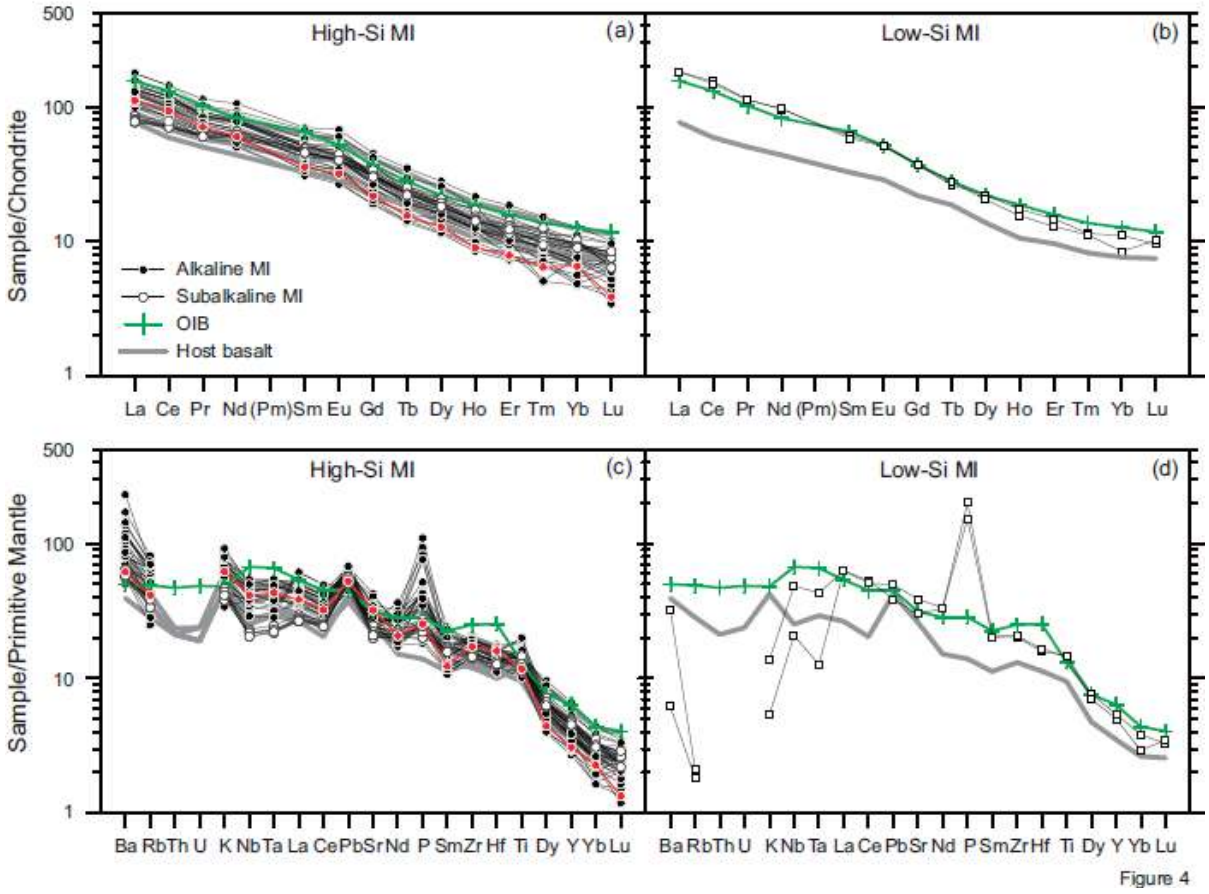

Figure 4

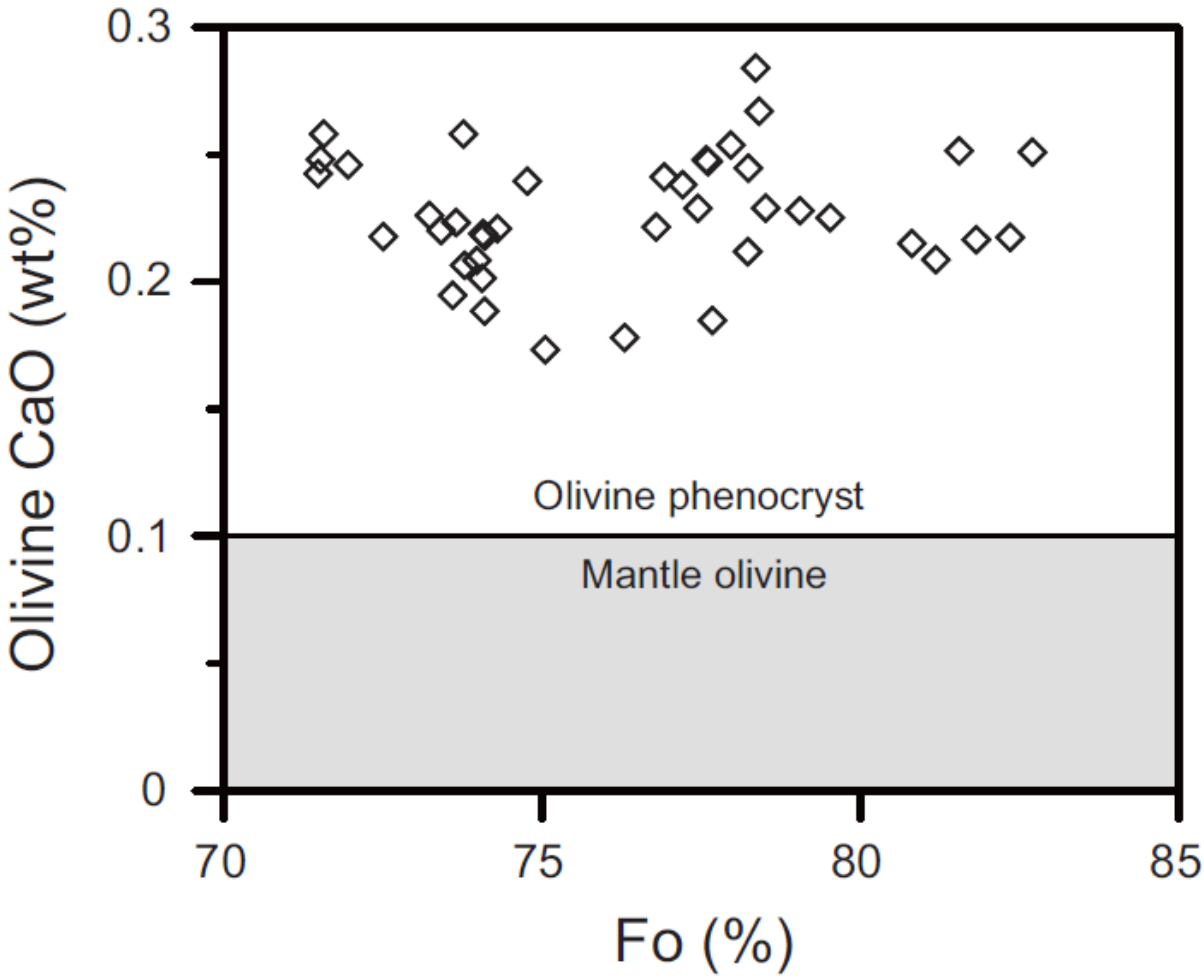

Figure 5

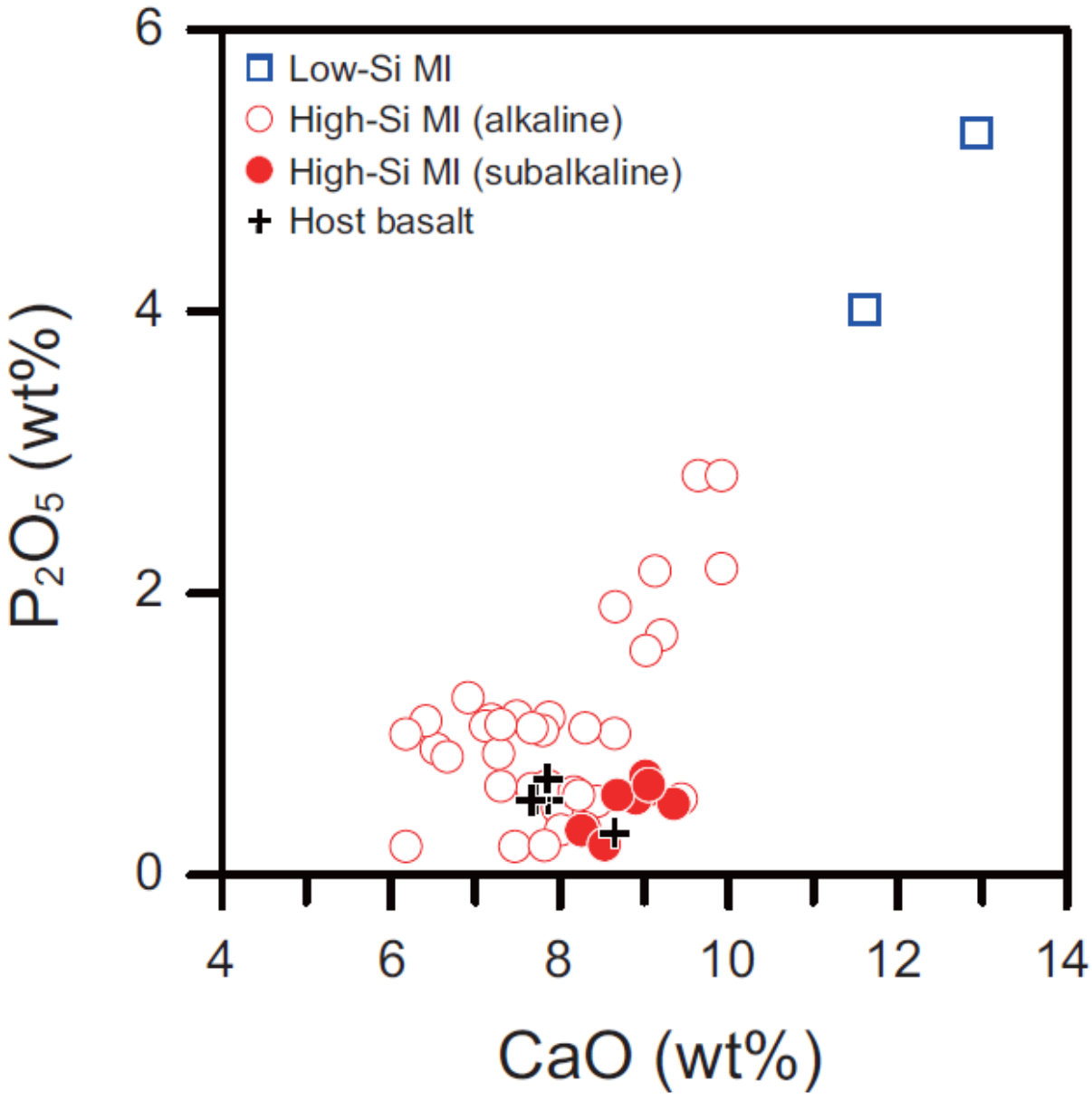

Figure 6

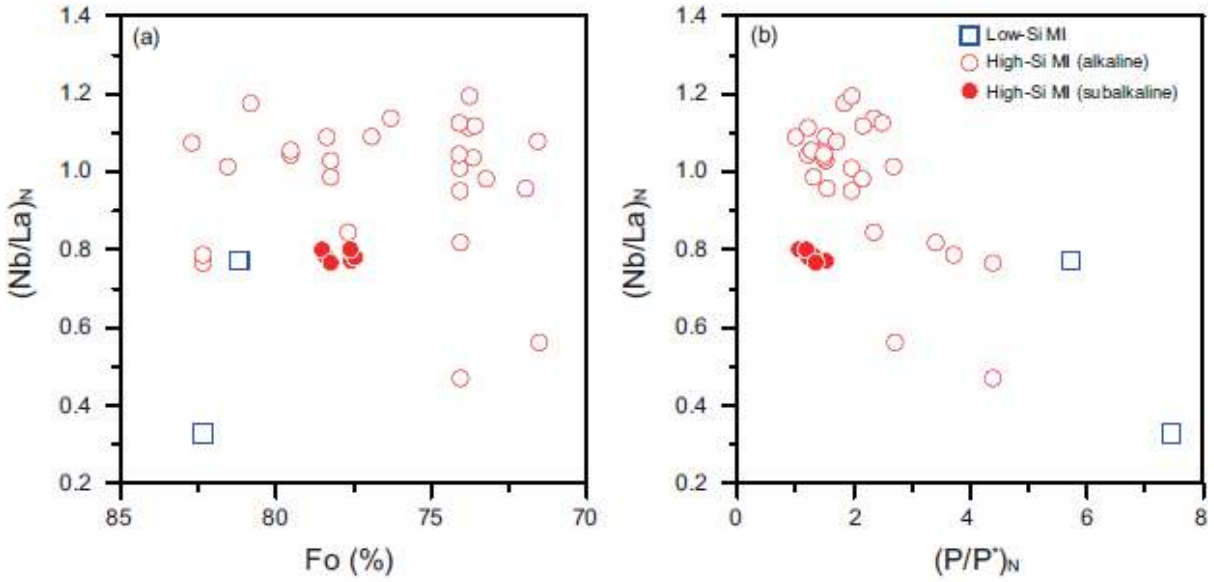

Figure 7

Figure 8

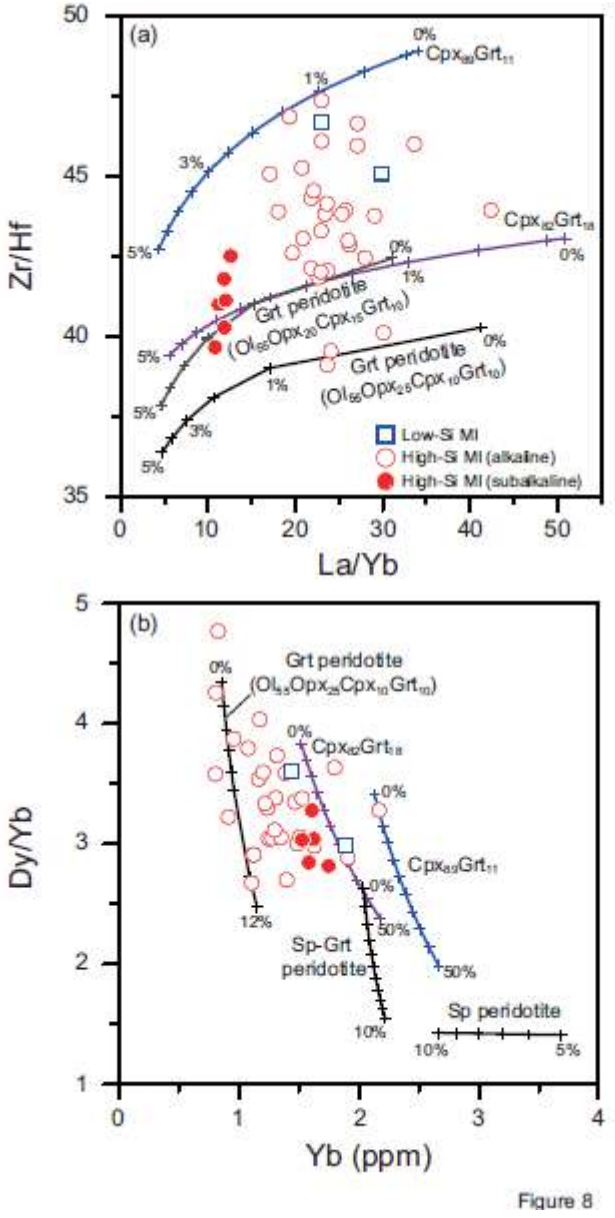

Figure 8

Figure 9

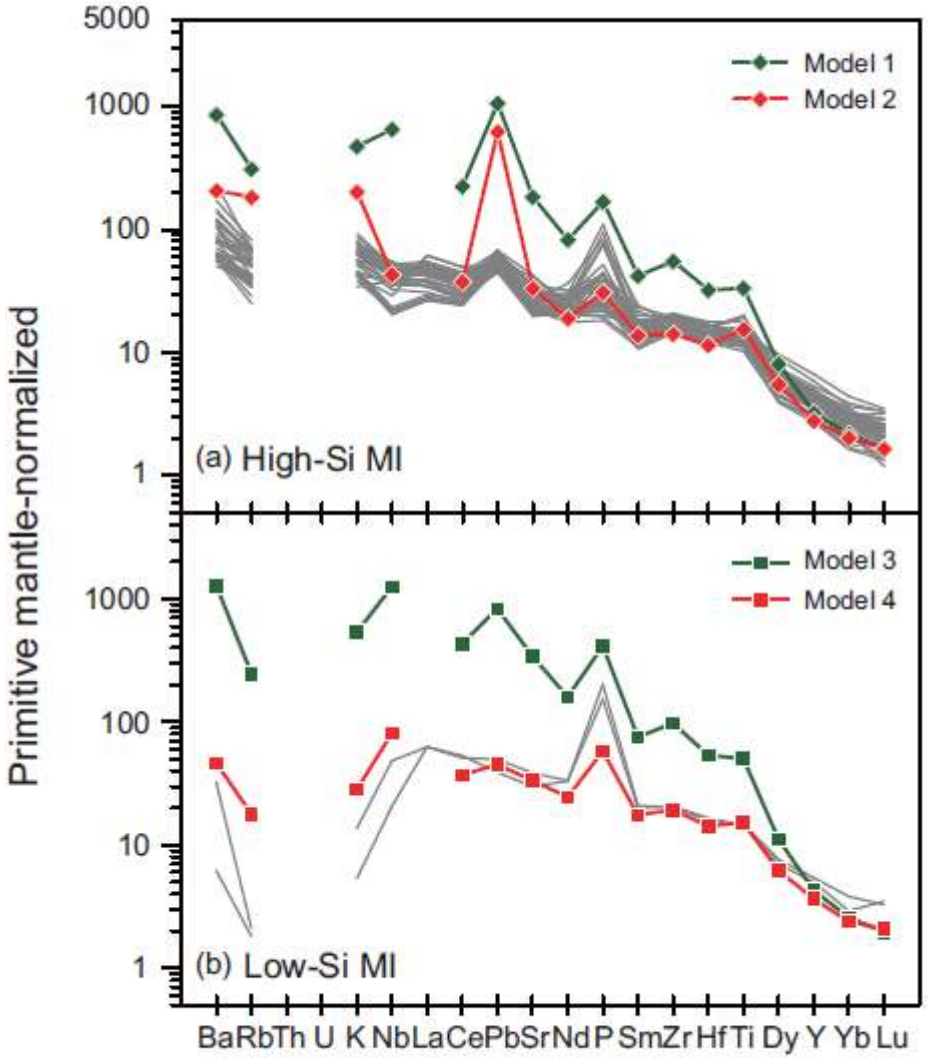

Figure 9

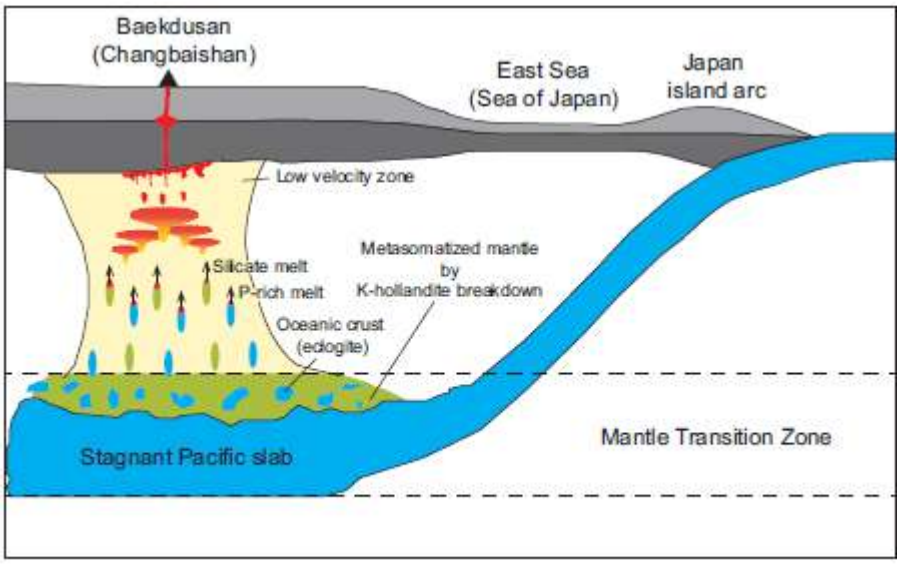

Figure 10